Article

Cell

Turbulence Activates Platelet Biogenesis to Enable Clinical Scale *Ex Vivo* Production

Graphical Abstract

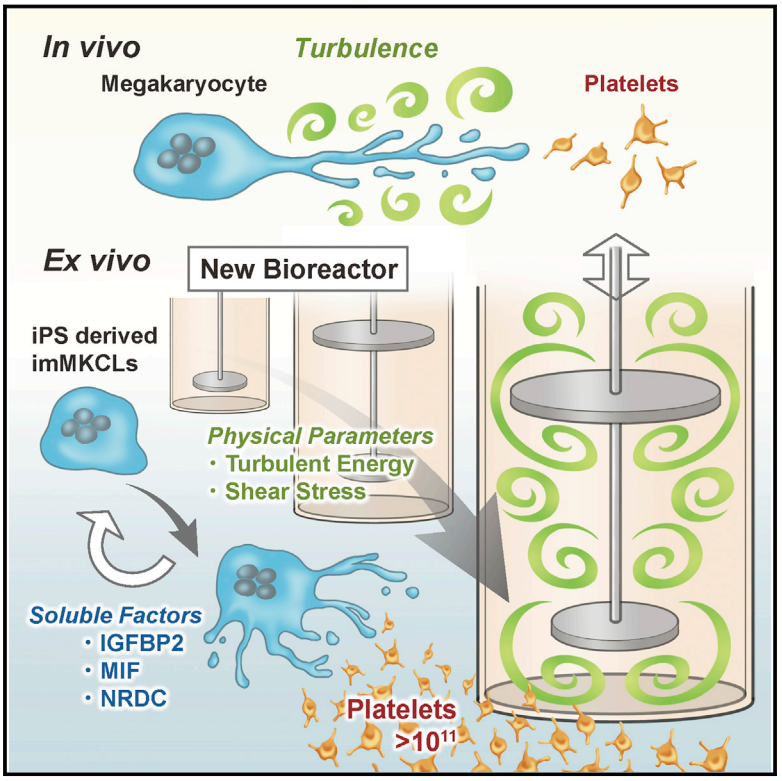

Highlights

- *In vivo* imaging revealed turbulence activates platelet biogenesis in mice
- Turbulent flow-based bioreactors enabled thrombopoiesis with high yield and quality
- Optimized turbulent energy along with shear stress are key parameters for scaling up
- Detection of cell-autonomous mechanism by the soluble factors IGFBP2, MIF, and NRDC

Authors

Yukitaka Ito, Sou Nakamura, Naoshi Sugimoto, ..., Fumihito Arai, Satoshi Nishimura, Koji Eto

Correspondence

kojieto@cira.kyoto-u.ac.jp

In Brief

Clinical-scale generation of platelets from human-induced pluripotent stem cells can be achieved in bioreactors when turbulence is factored in as an important physical regulator of thrombopoiesis.

Ito et al., 2018, Cell *174*, 636–648
July 26, 2018
https://doi.org/10.1016/j.cell.2018.06.011

CellPress

Cell

Article

Turbulence Activates Platelet Biogenesis to Enable Clinical Scale *Ex Vivo* Production

Yukitaka Ito,[1,10,13] Sou Nakamura,[1,13] Naoshi Sugimoto,[1] Tomohiro Shigemori,[10] Yoshikazu Kato,[11] Mikiko Ohno,[4] Shinya Sakuma,[6] Keitaro Ito,[6] Hiroki Kumon,[6] Hidenori Hirose,[10] Haruki Okamoto,[10] Masayuki Nogawa,[5] Mio Iwasaki,[2] Shunsuke Kihara,[3] Kosuke Fujio,[1] Takuya Matsumoto,[1] Natsumi Higashi,[1] Kazuya Hashimoto,[1] Akira Sawaguchi,[9] Ken-ichi Harimoto,[1,14] Masato Nakagawa,[2] Takuya Yamamoto,[2,12] Makoto Handa,[5] Naohide Watanabe,[5] Eiichiro Nishi,[4] Fumihito Arai,[6] Satoshi Nishimura,[7] and Koji Eto[1,8,15,*]

[1]Department of Clinical Application, Center for iPS Cell Research and Application (CiRA), Kyoto University, Kyoto, Japan
[2]Department of Life Science Frontiers, Center for iPS Cell Research and Application (CiRA), Kyoto University, Kyoto, Japan
[3]Department of Fundamental Cell Technology, Center for iPS Cell Research and Application (CiRA), Kyoto University, Kyoto, Japan
[4]Department of Pharmacology, Shiga University of Medical Science, Otsu, Japan
[5]Center for Transfusion Medicine and Cell Therapy, Keio University School of Medicine, Tokyo, Japan
[6]Department of Micro-Nano Systems Engineering, Nagoya University, Nagoya, Japan
[7]Center for Molecular Medicine, Jichi Medical University, Tochigi, Japan
[8]Department of Regenerative Medicine, Chiba University Graduate School of Medicine, Chiba, Japan
[9]Department of Anatomy, Faculty of Medicine, University of Miyazaki, Miyazaki, Japan
[10]Kyoto Development Center, Megakaryon Corporation, Kyoto, Japan
[11]Mixing Technology Laboratory, SATAKE Chemical Equipment Manufacturing Ltd., Saitama, Japan
[12]AMED-CREST, AMED, Tokyo, Japan
[13]These authors contributed equally
[14]Present address: Medical Devices & Materials Research Laboratory, Advanced Materials Research Laboratories, Toray Industries, Tokyo, Japan
[15]Lead Contact
*Correspondence: kojieto@cira.kyoto-u.ac.jp
https://doi.org/10.1016/j.cell.2018.06.011

SUMMARY

The *ex vivo* generation of platelets from human-induced pluripotent cells (hiPSCs) is expected to compensate donor-dependent transfusion systems. However, manufacturing the clinically required number of platelets remains unachieved due to the low platelet release from hiPSC-derived megakaryocytes (hiPSC-MKs). Here, we report turbulence as a physical regulator in thrombopoiesis *in vivo* and its application to turbulence-controllable bioreactors. The identification of turbulent energy as a determinant parameter allowed scale-up to 8 L for the generation of 100 billion-order platelets from hiPSC-MKs, which satisfies clinical requirements. Turbulent flow promoted the release from megakaryocytes of IGFBP2, MIF, and Nardilysin to facilitate platelet shedding. hiPSC-platelets showed properties of bona fide human platelets, including circulation and hemostasis capacities upon transfusion in two animal models. This study provides a concept in which a coordinated physico-chemical mechanism promotes platelet biogenesis and an innovative strategy for *ex vivo* platelet manufacturing.

INTRODUCTION

Blood transfusion is one the most common forms of cell therapy, with an estimated number of 4.5 million done annually in the United States alone (Whitaker and Hinkins, 2011). The transfusions depend on volunteers donating their blood, but in the near future, donor supplies are not expected to meet patient demand in several countries. In response, alternative platelet sources are being investigated (Stroncek and Rebulla, 2007).

Several groups including ours have proposed human-induced pluripotent stem cells (hiPSCs) as such a source, but the practical *ex vivo* manufacturing of 200–300 billion platelets, which is the number used for one transfusion, with the functional properties of bona fide circulating platelets has not yet been achieved (Takayama et al., 2010; Nakamura et al., 2014; Thon et al., 2014; Moreau et al., 2016; Sim et al., 2016). Better megakaryopoiesis and platelet shedding in hiPSC differentiation protocols are needed. The use of expandable and cryopreservable megakaryocyte cell lines established by the introduction of transgenes has been proposed for megakaryopoiesis (Nakamura et al., 2014; Moreau et al., 2016). We have shown that immortalized megakaryocyte cell lines (imMKCLs) derived from hiPSCs can be robustly expanded by the overexpression of c-MYC, BMI1, and BCL-XL, and doxycycline can be used to stimulate the proliferation (Dox-ON) and maturation (Dox-OFF) of the cells (Nakamura et al., 2014). As for platelet shedding, bioreactors that operate on the premise of only the shear stress observed in bone marrow (BM) (Junt et al., 2007; Zhang et al., 2012) have been proposed but have so far failed to achieve clinical scale manufacturing (Thon et al., 2014; Blin et al., 2016; Di Buduo et al., 2015; Nakagawa et al., 2013; Avanzi et al., 2016).

In the present report, we observe *in vivo* flow dynamics, finding that turbulent flow is a crucial physical factor for platelet release. Based on this finding, we developed a turbulent flow-based bioreactor, VerMES, by reciprocal vertical movement,

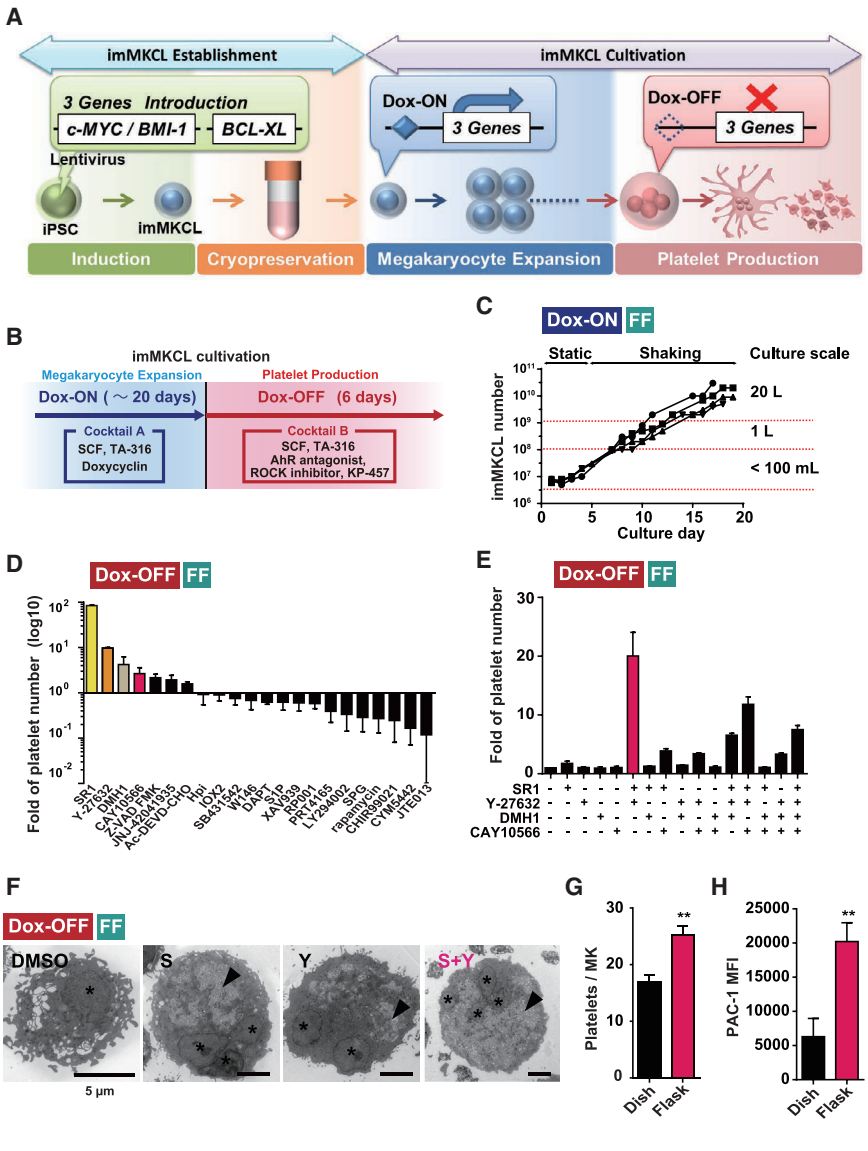

Figure 1. Establishment of Feeder-Independent Scalable Expansion and Maturation of imMKCLs

(A) Schema of the imMKCL system for platelet production. imMKCLs are established from human iPSCs by introducing three Dox-inducible transgenes, c-MYC, BMI-1, and BCL-XL, during megakaryocyte differentiation. A cryopreserved imMKCL stock is thawed and expanded by culturing with Dox (Dox-ON). Platelets are produced upon maturation by turning off the transgenes through the depletion of Dox (Dox-OFF).

(B) During imMKCL expansion phase and platelet production phase, media is supplemented with cocktail A (SCF, TA-316, and Dox) and cocktail B (SCF, TA-316 AhR antagonist, ROCK inhibitor, and KP-457), respectively.

(C) Numbers of $CD41a^+$ megakaryocytes (imMKCL Cl$^-$7) during expansion are shown. Approximately 10^7 imMKCLs were thawed and incubated in a Petri dish under static feeder cell-free (FF) conditions. The cells were grown in a flask, then in a 1-L scale WAVE bag and finally in a 20-L scale WAVE bag. Four independent experiments.

(D) Screening of drugs for platelet generation from Dox-OFF imMKCLs without feeder cells. The number of platelets produced without drugs was set to 1.0 (10^0). n = 3 experiments.

(E) Fold changes in $CD42a^+CD42b^+$ platelet numbers relative to those obtained without drugs. Platelets were obtained by several protocols using SR1, Y27632, DMH1, and/or CAY10566 along with TA316, SCF, and KP457. n = 3 experiments.

(F) Transmission electron micrographs of Dox-OFF imMKCLs with or without SR1 and/or Y-27632. Arrowheads, demarcation membrane systems; asterisks, nuclei; S, SR1; Y, Y-27632. Scale bars, 5 μm.

(G and H) Numbers of platelets generated per megakaryocyte (MK) (G) and MFI of bound PAC1 antibody after ADP and TRAP-6 stimulation (H) in a 10-cm Petri dish or 125 mL-scaled shaking flask. n = 3 experiments. **p < 0.01.

All data in (D), (E), (G), and (H) are means ± SD. See also Figure S1.

and identified turbulent energy as a physical parameter that assures consistent platelet yield independently of the reactor scale and culture volume. In addition, we found novel chemical factors in thrombopoiesis that contribute to the remodeling of mature megakaryocytes and shedding of platelets. Accordingly, platelets with the competency of bona fide platelets were produced efficiently in a scaled-up system at clinically relevant numbers.

RESULTS

Feeder-Independent imMKCL Culture System

For the *ex vivo* production of human platelets compatible with clinical application, we sought to develop a culture system that is independent of adherent feeder cells for imMKCLs (Figure 1A) (Nakamura et al., 2014). The expansion phase culture medium was supplemented with cocktail A, which includes doxycycline, stem cell factor (SCF), and TA-316, a thrombopoietin (TPO) mimetic small molecule (Aihara et al., 2017) (Figure 1B). In this phase, imMKCL numbers increased from 5×10^6 to 5×10^{10} in 15–20 days of culture, first in a rotating flask and then in a WAVE bag system by mild rocking movement (Figure 1C). The imMKCL showed stable proliferation for more than 70 days while retaining the $CD41^+CD42b^+$ phenotype (Figure S1A). Cocktail B in maturation phase culture medium includes an AhR antagonist, a ROCK inhibitor, and an ADAM17 inhibitor, KP-457 (Figure 1B). KP-457 maintains the surface expression of GPIbα (CD42b) ectodomain on platelets (Hirata et al., 2017). Because platelet release from Dox-OFF imMKCL in the medium with SCF and recombinant TPO originally required the presence of C3H10T1/2 mouse feeder cells (Figure S1B) (Nakamura et al., 2014), we screened candidate drugs (Figure 1D) and then found that an AhR antagonist, StemReginin1 (SR1) (Strassel et al., 2016), plus a ROCK

inhibitor, Y-27632 (Gobbi et al., 2013), most efficiently promoted platelet generation under feeder cell-free condition (Figure 1E). These generated platelets also showed the highest PAC-1 antibody binding capacity upon activation (Figure S1C). PAC-1 antibody binding capacity is a hallmark of platelet activation and indicates the activated form of the glycoprotein IIb/IIIa complex. Accordingly, Dox-OFF imMKCL with SR1 and Y-27632 developed the demarcation membrane system, a structural characteristic of mature megakaryocytes (Figures 1F and S1D). As for plasma content, 15% fetal bovine serum or 15% human serum has been used previously, but we found that 5% human plasma was sufficient for the maturation phase (Figure S1E). The lower human plasma content reduces cost and minimizes use of animal-derived components.

We also noticed that rotational shaking of a flask (E125 flask: 25 mL volume) resulted in higher platelet yield and better PAC-1 binding upon stimulation than did static conditions in a Petri dish (10 mL volume) (Figures 1G and 1H), suggesting that physical stress from horizontal shaking under liquid culture conditions further enhances platelet generation.

Turbulence in Thrombopoiesis *In Vivo*

For the bioreactor during the maturation of and final platelet release from imMKCLs, we initially tested a WAVE bag bioreactor, which is a rocking bag-based system (Figure S2A). However, while this system was capable of consistently proliferating imMKCLs at 20-L scale (cell division phase) (Figure 1C), the number and quality of platelets produced was very low. Further investigation led us to realize that the system lacked sufficient physical stress, as evidenced by the low values of several physical fluidic parameters (Figure S2B; Video S1).

It was previously proposed that blood flow-dependent shear stress is crucial for platelet biogenesis from mouse BM megakaryocytes (Junt et al., 2007). Based on several bioreactors that were developed in attempt to recapitulate this BM flow condition (Nakagawa et al., 2013; Thon et al., 2014; Blin et al., 2016), we developed a new bioreactor with a flow chamber and multiple pillars (Figures S2C and S2D). However, it too was unsatisfactory, as evidenced by the final yield of only 14 platelets per imMKCL (Figure S2E), far short of the 500–1,000 platelets per megakaryocyte assumed in the mouse body (Lefrançais et al., 2017). Thus, whether shear stress alone is the determinant fluid dynamic factor in platelet shedding is unclear. To examine the ideal physical conditions for platelet biogenesis, we conducted *in vivo* live observations. To analyze and visualize dynamic blood flow during platelet release *in vivo*, we performed two-photon microscopy and particle image velocimetry (PIV) of BM from the scalps of eGFP mice (Figure 2A) (Nishimura et al., 2015). Active megakaryocytes (large cells with high eGFP-expressing cytoplasm) displayed proplatelets and shed platelet particles that were adjacent to differentially directed dynamic flow vectors, indicating high turbulence was present around moving proplatelets (Figures 2B and 2C; Videos S2 and S3). In contrast, resting megakaryocytes that did not release platelets were exposed to continuous laminar flow patterns with no turbulence (Figure 2D; Video S4). We interpreted these observations to indicate dynamic blood flow with turbulence is crucial for platelet generation (Figure 2E).

Turbulence Induces *In Vitro* Thrombopoiesis

Simulation analysis revealed that the flow in the WAVE system lacked sufficient levels of shear, vorticity, or turbulent energy (Figure S2B; Video S1). Our new microfluidic system produced appropriate levels of shear stress (Pa) at a high shear rate (s^{-1}) in laminar flow with vorticity only around the pillars, but no turbulence due to the microfluidic structure (Figure S2D). After thorough testing and simulation of agitated flow in various devices, we found VerMES, a vertical reciprocal motion type liquid culture bioreactor, is effective at platelet generation. The 2.4 L VerMES bioreactor includes two oval-shaped mixing blades fixed at a horizontal angle to the power axis and at right angles to each other. The blades repeat an up-and-down reciprocal motion at a maximum speed of 300 mm/s to generate turbulent flow (Figures 3A and S3A). We found $CD41^+CD42b^+$ platelet particle generation in a static Petri dish and 20-L WAVE bag reactor was <20 platelets per imMKCL, but in the 2.4 L VerMES at 120 or 300 mm/s it was ~70–80 platelets per megakaryocyte (Figure 3B). Moreover, the platelets generated in the VerMES bioreactor at these speeds showed high PAC-1 binding upon activation (Figure 3C) and lower annexin V binding at steady state (Figure 3D), indicating proper activation capacity and low deterioration due to pre-activation or aging.

Furthermore, simulation analysis revealed that the VerMES system bore sufficient levels of turbulence, vorticity, and shear (Figures 3E and S3B; Video S5). To identify the determinant parameters that correlate with the improved generation of intact platelets between differently sized bioreactors, we examined the yield of functional $CD41^+CD42b^+$ platelets at a broad range of reciprocal motion speeds using the single-bladed 0.3 L VerMES (Figure S3C; Video S5). At this scale, 100–250 mm/s reciprocal motion speed was optimal for platelet yield (Figure S3D). We then plotted the values of platelet productivity with the following parameters: turbulent energy, vorticity, shear stress, and shear strain rate for the 0.3 L and 2.4 L VerMES (Figures 3F–3I). We found that the relationship between turbulent energy (Figure 3F) and shear stress (Figure 3H) for the generation of functional platelets was the same at the two different volumes, but this was not the case for vorticity (Figure 3G) or shear strain rate (Figure 3I). These results indicate that optimized levels of turbulent energy (0.002–0.014 m^2/s^2) as well as shear stress (0.4–3.0 Pa) reflect efficient platelet generation in physical stress conditions with turbulence independently of the VerMES scale size. Indeed, by adjusting to the identified optimal range of turbulent energy and shear stress in the 8 L VerMES (stroke, 40 mm; speed 150 mm/s), we succeeded in obtaining ~100 billion platelets using three imMKCL clones (Figure 3J). In addition, the quality of the produced platelets was comparable to those seen at the 2.4-L scale, as exemplified by low annexin V binding (Figure 3K) and the high percentage of $CD42b^+$ platelets (Figure 3L). Additionally, platelet antigens were highly expressed (Figure S3E), and P-selectin expression and PAC-1 binding were properly induced upon 100 μM ADP and 40 μM TRAP-6 stimulation (Figures S3F and S3G).

Functionality of iPSC-Platelets

We next processed the platelets generated in VerMES to final product form and evaluated their functionality. To prepare

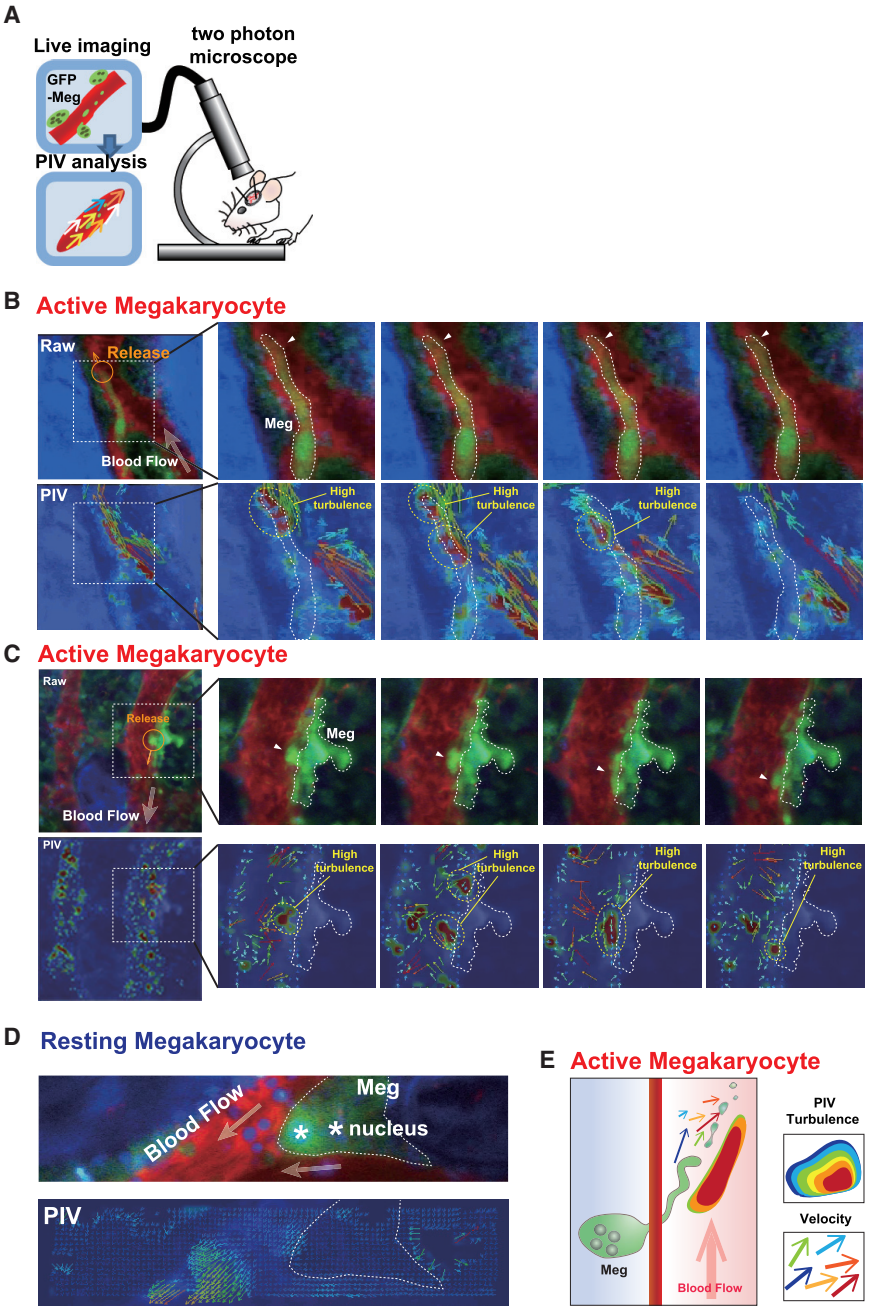

Figure 2. *In Vivo* Imaging Shows Turbulent Flow Dependency of Platelet Biogenesis from Mouse Bone Marrow Megakaryocytes

(A) Schema of the *in vivo* imaging. Blood flow around bone marrow (BM) megakaryocytes (Meg) expressing GFP in the mouse scalp were subject to time-lapse imaging with particle imaging velocimetry (PIV) analysis.

(B) Active thrombopoiesis in living BM from 6-week-old CAG-eGFP mice (×400). Scale bar, 50 μm. Red (Texas-red-dextran), blood flow; GFP, megakaryocytes; blue (Hoechst33342), bone area and nucleated cells. Left: orange circles and arrows mark platelet release. Translucent arrows: direction of blood flow. Dotted square areas are expanded in the four time-lapse images to the right. In the raw and PIV time-lapse images, megakaryocytes are indicated by dotted lines and arrow heads show platelet shedding from proplatelets. Flow rate and directions are marked by PIV vectors (red, fast; blue, slow). Turbulence is qualitatively measured (red, high; blue, low) and marked by yellow dotted circles. PIV, images analyzed by PIV. See also Video S2.

(C) Another example of active megakaryocytes in mouse bone marrow (×400). Conventions are the same as in (B). See also Video S3.

(D) Resting Meg without platelet shedding are seen in the area without turbulence. Conventions are the same as in (B) and (C) (×400). Scale bar, 20 μm. See also Video S4.

(E) Schema of an active megakaryocyte. Dynamic flow indicated by various directed arrows and high turbulence indicated by red were observed near the platelet shedding site.

See also Figure S2 and Video S1.

iPSC-platelets (imMKCL-derived platelets) in ACD-containing bicarbonate Ringer's solution (i.e., washed-type concentrate) (Oikawa et al., 2013), hollow fibers were used in combination with a centrifugation system to wash and purify platelets in Dox-OFF culture suspension from the 8 L VerMES on day 6 (Figure 4A). Although the final suspended platelets were larger and the sizes varied with the imMKCL clones (3–8 μm; Figure S4A), iPSC-platelets had intact structures including alpha-granules consistent of circulating platelets (Figures 4B and S4B).

We then examined the *in vitro* and *in vivo* functionality of the washed iPSC-platelet concentrates. Human donor platelets gradually lose their aggregation capacity, which is one reason why they have a shelf-life limit of only 5 days in the United States (D1 is the day blood is taken from the donor). Fresh D1 iPSC-platelets aggregated similarly to pooled donor platelets in platelet aggregation assays (Figure 4C). PAC-1 binding along with P-selectin expression upon stimulation were also consistent with donated platelets (Figure 4D). Likewise, iPSC-platelets functioned comparably to D3 donor platelets in clot retraction assays (Figure S4C), exhibiting granule release, as measured by platelet factor 4 (PF4) and β-thromboglobulin (βTG) concentrations (Figures S4D and S4E), and platelet spreading on fibrinogen after agonist stimulation, which represents outside-in signaling from integrin αIIbβ3 (Figure S4F) (Takizawa et al., 2010). Interestingly, the kinetics in NOG mice revealed a transient increment in the peripheral blood platelet count for 4 hr after the transfusion of iPSC-platelets derived from the $Cl^{-}7$ clone, but not for those derived from the N5-6 clone, MK04 clone, or donor platelets (Figures 4E and 4F). This transience may be because the large-sized $Cl^{-}7$ iPSC-platelets fractionate into smaller platelets after

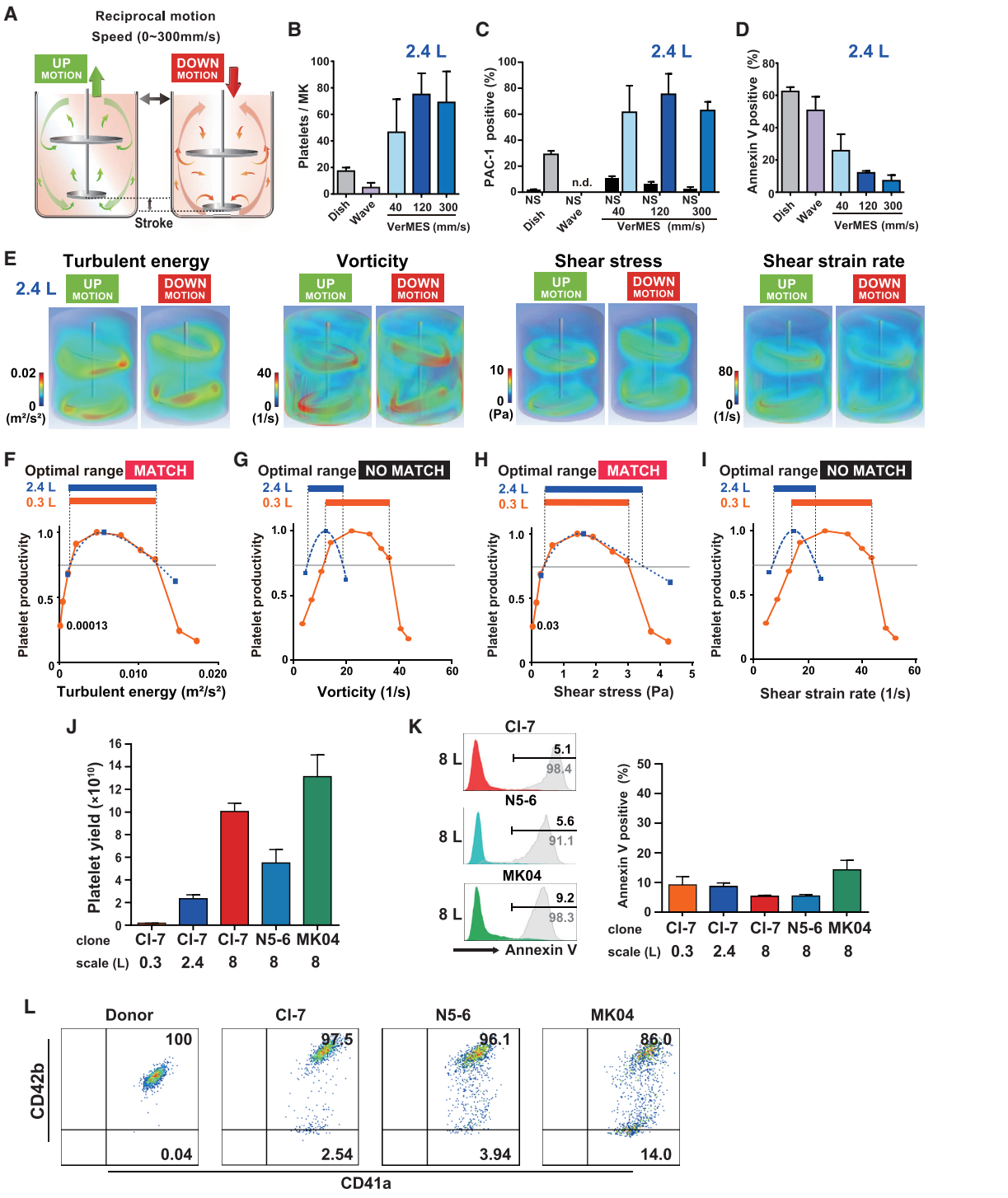

Figure 3. Optimal Shear Stress and Turbulent Energy in the VerMES Bioreactor Enables Scalable Platelet Biogenesis

(A) Schema of the VerMES bioreactor.

(B) Numbers of platelets generated per megakaryocyte (MK; imMKCL Cl⁻7) in a Petri dish, 20 L WAVE bioreactor, and 2.4 L VerMES with 30 mm strokes at the indicated speeds. n = 2–5 experiments.

(C and D) Ratio of platelets bound with PAC1 antibody after 100 μM ADP and 40 μM TRAP-6 stimulation (C) or Annexin V binding in the unstimulated state (D) quantified using flow cytometry. n.d., not detected; NS, not stimulated. n = 2–5 experiments.

(E) Simulation results during up and down reciprocal motion with the indicated physical parameters in 2.4 L VerMES bioreactor.

(legend continued on next page)

transfusion (Figures S4A and S4G). Consistent with that idea, the peak forward scatter of Cl⁻7 iPSC-platelets prior to injection was nearly 3 times higher than the peaks at post-injection time points (0.5, 1, 2, 4, and 6 hr) (Figure S4H).

Finally, we evaluated hemostatic functionality *in vivo*. Measurements of bleeding time were performed in thrombocytopenic animal models. In the NOG mouse model (Nakamura et al., 2014), bleeding times following the transfusion of platelets derived from the three different clones (24 hr post preparation in Figure 4A) or day 3 (48 hr after taken) donor platelets were comparable (Figures 4G and 4H). Two photon microscopic observations of platelets labeled with red fluorescent dye (TAMRA) following thrombotic occlusion induced by laser injury revealed that the thrombus formation was stable in both donor- and iPSC-platelets even against strong blood flow speed in a large vessel (diameter >100 μm) (Figure 4I; Video S6). This thrombus formation was observable only in microvessels with slower blood flow speed in our earlier study of iPSC-platelets (Nakamura et al., 2014). Further, in a recently established rabbit model, which shows high sensitivity for the hemostatic function of stored human platelets (Figure 4J) (Watanabe et al., 2017), iPSC-platelets (Cl⁻7) induced hemostasis similarly to donor platelets within the shelf-life limit of 5 days (96 hr), as indicated by bleeding times (Figure 4K) and the complete hemostasis rate (Figure 4L). The post-transfusion kinetics in the rabbit model was similar to that in the NOG mouse model (Figures S4I and S4J). Therefore, iPSC-platelets generated through our *ex vivo* production protocol exhibited better functionality than platelets produced using feeder cells in a Petri dish and performed close to the level of donor platelets, including hemostatic and circulating activity *in vivo* (Nakamura et al., 2014).

imMKCL-Derived Thrombopoietic Mediators

We next addressed how the optimized VerMES bioreactor increased the efficiency of intact platelet generation at the molecular level. There were no obvious differences in the global gene expression profiles of imMKCL populations derived under static or VerMES conditions (Figure S5A). Platelet generation was increased in the flask-shaking condition if the medium was changed on day 3 of the 6-day culture to the culture supernatant obtained from optimized 2.4 L VerMES culture, but no change was seen if the change was to fresh medium with cocktail B (Figures S5B and S5C). Interestingly, culture medium conditioned in the VerMES did not appear to promote platelet generation in a Petri dish static condition (Figure S5C). Regarding annexin V binding levels, physical flask shaking was sufficient to achieve low levels even without changing the conditioning medium (Figure S5D), suggesting the effect of physical stress on intact platelet shedding. Considering that the levels of shear stress and turbulent energy in a shaking flask were 50% and 40%, respectively, of those achieved in optimized VerMES (Figure S5E), these results suggest soluble mediators present under VerMES-applied conditions positively influence platelet generation only in the presence of flow, and that turbulence in the VerMES enhances the release of these mediators.

We identified candidate soluble mediators by using a protein array to assess the difference in cytokines between culture medium specimens from dishes and VerMES (4-day incubation of imMKCLs with Dox-OFF) (Figure S5F). Through this approach, we selected five candidate factors: insulin growth factor binding protein 2 (IGFBP2) (Coppé et al., 2008), macrophage migration inhibitory factor (MIF) (Strüßmann et al., 2013), chemokine (C-C motif) ligand 5 (CCL5, or RANTES) (Machlus et al., 2016; Tamura et al., 2016), thrombospondin-1 (TSP-1) (Lim et al., 2008), and plasminogen activator inhibitor-1 (PAI-1) (Madoiwa et al., 1999) (Figure 5A). We also assessed nardilysin (NRDC) (Nishi, 2013), which we previously observed to affect platelet yield. NRDC was expressed markedly higher in the VerMES condition according to ELISA analysis (Figure 5A). Among these six factors, the levels of NRDC, IGFBP2, and CCL5 were upregulated by SR1 plus Y27632 for the maturation of imMKCL (Figure S5G). Of these three, NRDC was particularly upregulated in optimized VerMES. Similar to VerMES culture conditioned medium (Figure S5C), the addition of recombinant forms of the six factors into fresh medium (MIF: 10 ng/mL, other 5 factors: 50 ng/mL) resulted in significantly higher platelet yields in shaking flasks (Figures 5B and 5C), which have about half the level of shear stress and turbulent energy as VerMES (Figure S5E), suggesting strong thrombopoietic effects in the VerMES conditioned media.

To determine the actions of each mediator, we removed each factor from the group of six factors and observed the effect on platelet biogenesis in the aforementioned microfluidic system, which generates high shear stress but no turbulence and can form proplatelets but releases low numbers of platelets (Figures S2C–S2E). While the administration of the six factors into the fluidic system increased the platelet yield, overall results suggested that MIF, IGFBP2, and NRDC are crucial (Figure 5D). Indeed, these three factors were most secreted at the optimal flow speed of VerMES (Figure S5H), and their administration alone significantly increased platelet generation in the flasks (Figure S5I).

Notably, in preparations without IGFBP2 or MIF in the microfluidic system, most imMKCLs and proplatelets failed to adhere

(F–I) Correlation between platelet productivity and calculated turbulent energy (F), vorticity (G), shear stress (H), and shear strain rate (I) using 0.3 L (orange circles, n = 3–15 experiments in 10 conditions, see Figure S3D) or 2.4 L (blue squares, n = 2–5 experiments in 3 conditions) VerMES. Maximum productivity was defined as 1.0. Range of optimal platelet productivity in each scaled VerMES compared to flask culture is shown.

(J) CD41-positive platelet yield in VerMES under optimal conditions from imMKCL clones Cl⁻7 (0.3 L, 2.4 L, and 8.0 L scale), N5-6 (8.0 L scale), and MK04 (8.0 L scale). n = 3 experiments.

(K) Annexin V bound to CD41-positive platelets derived from the indicated imMKCL clones using VerMES. Representative histograms are shown in left panels. Histograms stimulated with ionomycin (ash color) are overlaid. n = 3 experiments.

(L) Representative dot plots from flow cytometric analyses showing the expression of CD41a and CD42b on platelets from healthy donor or on iPSC-platelets from imMKCL clones Cl⁻7, N5-6, and MK04.

See also Figure S3 and Video S5.

All data in (B)–(D), (J), and (K) are means ± SD.

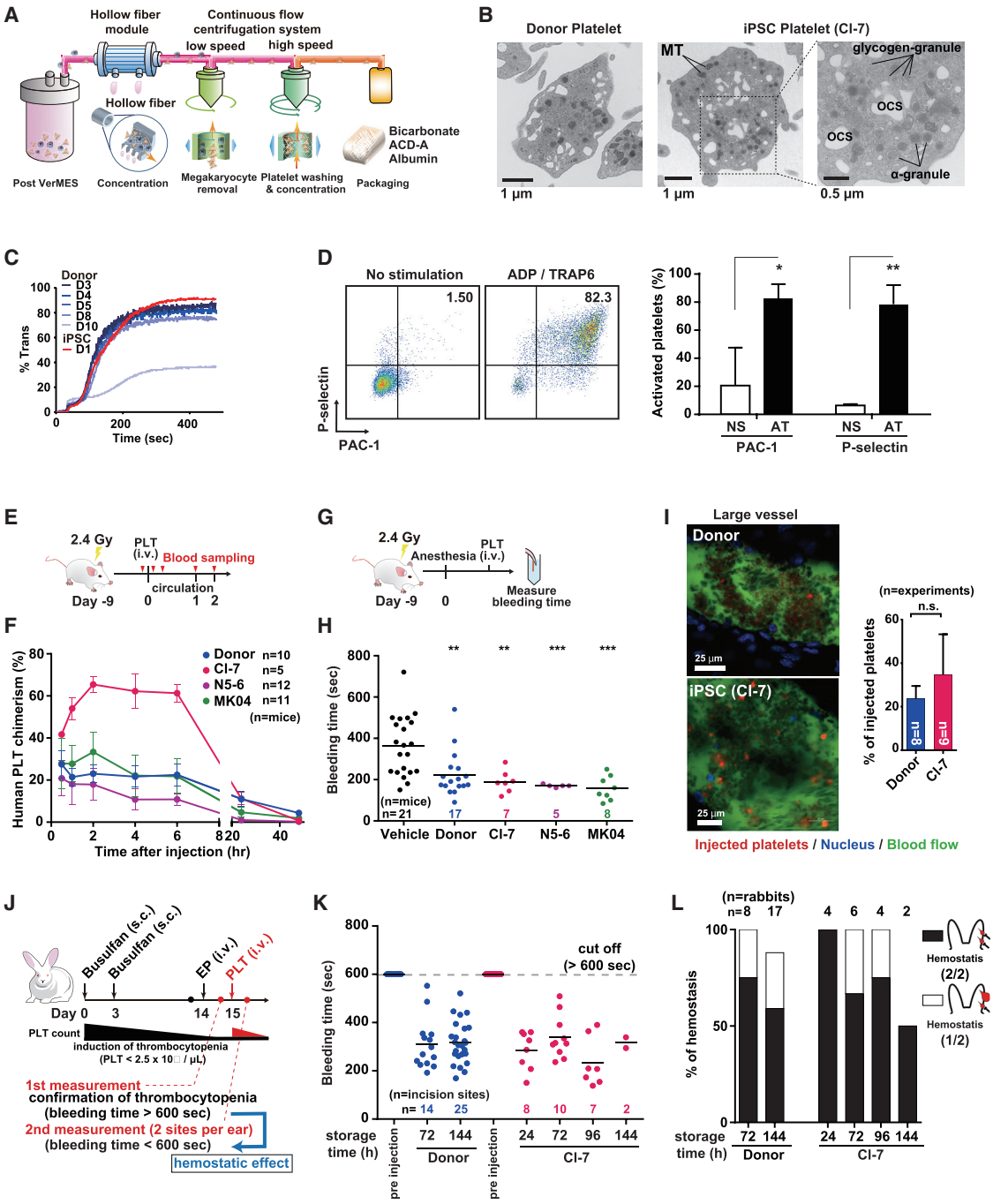

Figure 4. iPSC-Platelets Generated in the VerMES Bioreactor Improved Thrombotic Responses *In Vitro* and *In Vivo*

(A) Schema for processing washed-type platelets. Hollow fiber filtration was used to reduce the VerMES volume from 8 L to 1-2 L, followed by removal of the remaining imMKCLs by continuous centrifugation. Eventually, washed platelets were resuspended in platelet storage solution consisting of bicarbonate Ringer's solution with 5% ACD-A solution plus 2.5% human serum albumin.

(B) TEM images of donor and imMKCL-derived platelets (Cl⁻7) produced in VerMES. MT, mitochondria; OCS, open canalicular system. Scale bars, 1 μm and 0.5 μm.

(C) Aggregation assay. Day 1 (D1) corresponds to the collection day of donor platelets and preparation day of iPSC-platelets. Platelets were stimulated with 5 μg/mL collagen and 10 μM ADP.

(D) PAC-1 binding and P-selectin expression on washed-type iPSC-platelets without stimulation (NS) or with 100 μM ADP and 40 μM TRAP-6 (AT). Left: representative dot plots. Right: n = 3 experiments. *p < 0.05, **p < 0.01.

(legend continued on next page)

at the pillars (Figure 5E; Video S7), suggesting these two mediators regulate anchoring to extracellular matrix (ECM) components (Abbonante et al., 2017; Dunois-Lardé et al., 2009; Larson and Watson, 2006; Pallotta et al., 2009; Poirault-Chassac et al., 2013; Strassel et al., 2009; Takizawa et al., 2008). When we examined intracellular ECM levels within cultured Dox-OFF imMKCLs after the addition of six or five factors (MIF-minus or IGFBP2-minus) (Figure 5F), the intracellular expressions of von Willebrand factor (vWF) and vascular cell adhesion molecule-1 (VCAM-1) were observed to be higher with the 5-factor condition (Figure 5G). In addition, the intracellular expressions of fibrinogen, fibronectin, vitronectin, and collagen IV were also higher with the 5-factor condition (Figure S5J). These results strongly indicate MIF and IGFBP2 induce the direct release of ECM from imMKCLs to help the anchoring of imMKCLs to the pillars of the microfluidic chamber.

In the microfluidic system that lacked turbulence, NRDC-minus cocktail mediated the elongation of proplatelets, but without apparent platelet shedding (Figure 5E; Video S7). Accordingly, knocking down endogenous NRDC in imMKCLs using an miRNA construct slightly diminished platelet generation (Figures S6A and S6B), and replacing NRDC with enzyme-inactivated NRDC (Glu235 to Ala mutant; E > A) (Hiraoka et al., 2008) reduced platelet generation in the six-factor condition (Figures 5D and 5E; Video S7). We concluded that the zinc-metalloendopeptidase activity of NRDC likely contributes to platelet shedding, but only in the presence of shear stress. We thus visualized the direct binding of extracellular NRDC at the putative shedding sites of proplatelets in the microfluidic system (Figure 6A). Super-resolution microscopy (STORM) analysis revealed aggregation spots of extracellular NRDC on elongated proplatelets expressing β1 tubulin, suggesting NRDC acts extracellularly to promote platelet shedding (Figure 6B). Therefore, NRDC may use its zinc-metalloendopeptidase activity to sever interactions with crucial shedding sites within proplatelets or the fragmented cytoplasm from megakaryocytes (Thon et al., 2010).

Because NRDC also acts as a shuttling protein and epigenetic regulator (Nishi, 2013), we performed immunoprecipitation in combination with mass spectrometry for NRDC in imMKCLs to identify its intracellular binding proteins. The analysis revealed that endogenous NRDC is specifically bound to α4A and β1 tubulins (Figure 6C). Immunohistochemical staining for α and β1 tubulins in mature imMKCLs showed their colocalization (Figure S6C). We then determined the intracellular localization of NRDC. Over the course of imMKCL maturation from day 1 to day 5, NRDC dislocated from the nucleus and was confined to the area below the plasma membrane to colocalize with α tubulin (Figure 6D). Because NRDC reportedly binds to HDAC3 (Li et al., 2012) and another HDAC family protein, HDAC6, regulates tubulin remodeling by deacetylation (Hubbert et al., 2002), we asked whether NRDC associates with HDAC6 in imMKCLs to affect platelet generation. We observed the co-localization of NRDC, α-tubulin, and HDAC6 in a sub-membrane area of imMKCLs and proplatelets (Figure 6E). The close proximity (<40 nm distance) of NRDC and HDAC6 in the cytoplasm of mature imMKCL was also confirmed by Duolink proximity ligation assay, while NRDC knockdown diminished the spots that represent their co-localization (Figure 6F). Furthermore, the addition of an HDAC6 inhibitor, nexturastat A (2 μM), completely blocked platelet generation under shaking (Figure 6G). These results indicate intracellular NRDC interacts with HDAC6 to regulate tubulin remodeling through deacetylation/acetylation (Hubbert et al., 2002; Miyake et al., 2016) and contributes to further platelet shedding in imMKCLs in our *ex vivo* system.

DISCUSSION

Based on the novel concept of turbulence in platelet biogenesis, we established a clinical scale *ex vivo* manufacturing system of bona fide type platelets from iPSC-derived imMKCLs. Our *in vivo* observations within mouse BM clarified the crucial involvement of turbulent flow in platelet biogenesis (Figure 2). Through the development of a turbulent flow-based scalable bioreactor, VerMES, we dramatically improved the yield and quality of platelets. Further, by identifying turbulent energy as a physical parameter for efficient platelet yield independent of cultivation scale size, the generation of 100 billion intact platelets (i.e., lowered Annexin V binding levels, which is similar

(E) NOG mouse circulation model. 2 × 10^8 imMKCL-derived or donor platelets were transfused into irradiated NOG mice. 2.4 Gy irradiation was performed at −9 days. Blood sampling was done prior and 0.5, 1, 2, 4, 6, 24, and 48 hr after injection.
(F) Flow cytometric analysis of the time course of chimerism in peripheral blood. n = numbers of mice.
(G) NOG mouse hemostasis model prepared like in (E).
(H) Bleeding times for vehicle, donor platelets, or iPSC-platelets. Horizontal bars represent averages. Statistical analyses were done by Mann-Whitney U test compared to vehicle. n = numbers of mice. **$p < 0.01$, ***$p < 0.001$.
(I) Representative two photon microscopic images and platelet content of a thrombus formed with donor platelets or iPSC-platelets within a large vessel. FITC-dextran (green), Hoechst 33342 (blue), and TAMRA-labeled platelets were transfused into mice (×1,000). n = numbers of experiments (numbers in graph). Scale bar, 25 μm.
(J) Rabbit hemostasis model. On day 0 and 3, busulfan was injected subcutaneously (s.c.) to induce thrombocytopenia. On day 14, ethylpalmitate (EP) was injected intravenously (i.v.) to block phagocytosis. On day 15, rabbits with platelet counts less than 2.5 × 10^4 /μL and bleeding from an incision site in the ear vein for over 600 s (1st measurement) were subject to the transfusion of platelets from blood donors or from imMKCL Cl⁻7 and assessed for hemostasis (2nd measurement). For 2nd measurement, bleeding was measured from two incision sites in the ear vein per rabbit.
(K) Bleeding times for donor platelets or iPSC-platelets in which hemostasis was observed within 600 s. Horizontal bars represent averages. Storage time indicates hours after product packaging. n = numbers of incision sites.
(L) The ratio of rabbits with hemostasis at 2 sites (2/2) or 1 site (1/2) per two incision sites. n = numbers of rabbits.
All data in (D), (F), and (I) are means ± SD.
See also Figure S4 and Video S6.

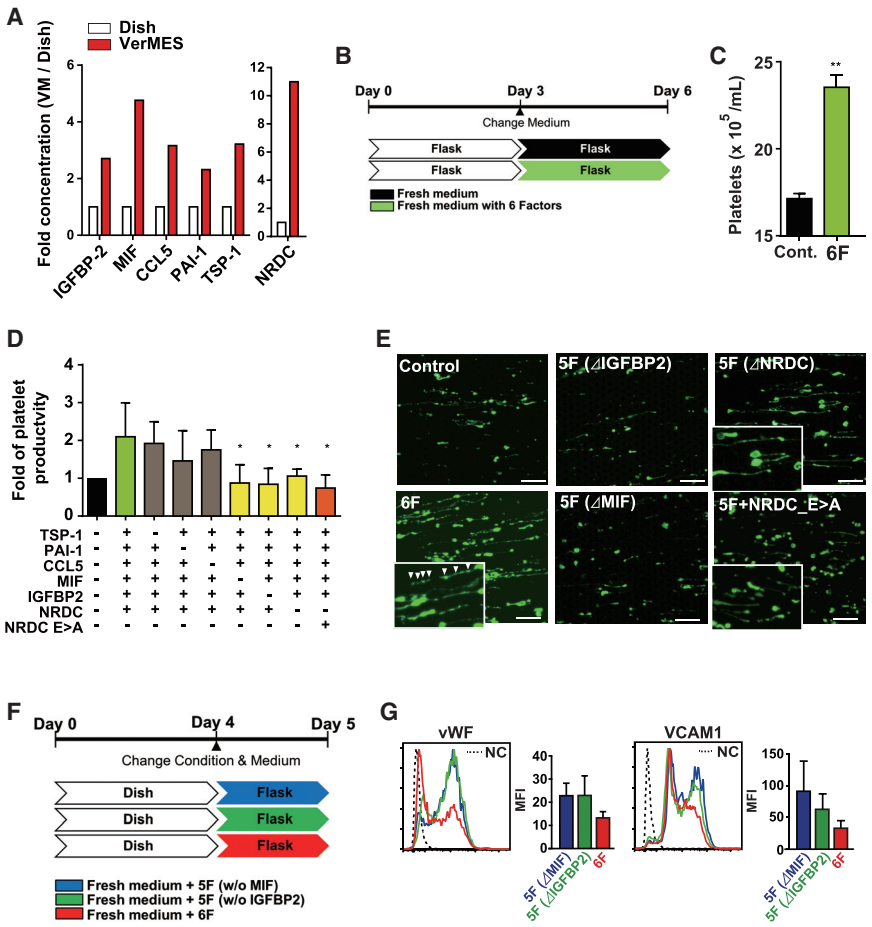

Figure 5. VerMES Cultivation Induced Release of Thrombopoietic Factors from imMKCLs

(A) Levels of the indicated 6 factors in imMKCL culture supernatants from dish or 2.4 L VerMES. The dish condition was set to 1.0. IGFBP-2, MIF, CCL5, PAI-1, and TSP-1 were quantified from protein array analysis images, and NRDC from ELISA. One of data from two independent experiments.

(B) To generate platelets, imMKCL were cultured in a flask with Dox-OFF medium for 3 days, then in fresh medium with or without 6 factors and cultured 3 more days in a flask (MIF: 10 ng/mL, other factors: 50 ng/mL).

(C) Numbers of $CD41^{+}CD42b^{+}$platelets generated from imMKCL ($Cl^{-}7$) in each condition shown in (B). n = 3 experiments.

(D) Platelet productivity in the micro fluidic system with the addition of the indicated factors by flow cytometric analysis. Control was set to 1.0. n = 3–5 experiments in each group. Statistical analyses were done by Dunnett's test compared to the six factors condition (6F). *p < 0.05.

(E) Representative pictures of imMKCLs in the microfluidic system with the addition of the indicated factors on day 5 of Dox-OFF condition (×100). Scale bars, 100 μm.

(F) Flow cytometric analysis of intracellular ECM. imMKCL cultured in a dish with Dox-OFF medium for 4 days, then changed to fresh medium with 6 factors or 5 factors (without MIF or IGFBP2) and cultured 1 more day in a flask.

(G) Representative histograms and bar graphs of mean fluorescence intensity (MFI) for intracellular ECM (vWF and VCAM1) levels in imMKCLs. Dotted lines in histograms indicate negative control (NC). n = 3 experiments.

All data in (C), (D), and (G) are means ± SD.

See also Figure S5 and Video S7.

to donor platelets) at 8-L scale was achieved, whereas Annexin V binding was over 60% in platelets from a Petri dish or a WAVE bag (Figure 3). Finally, the platelets when purified and resuspended to the specification of donor-derived washed platelet concentrate showed functionality comparable with donor platelets in two animal models, including one rabbit model approved by the Food and Drug Administration (FDA) (Figure 4) (Watanabe et al., 2017). The enhanced yield was due in part to the release of six crucial thrombopoietic chemical mediators from megakaryocytes (Figure 5). As a result, we demonstrated the unresolved molecular mechanisms of platelet shedding from mature megakaryocytes for the first time.

To promote platelet production from hiPSC-derived megakaryocytes, we initially adopted a microfluidic system that generates shear stress and vorticity, but the yield was unsatisfactory (Figures S2C–S2E). Accordingly, turbulent energy, which reflects the size of velocity fluctuations, was identified as the determinant parameter in the VerMES bioreactor. For the generation of turbulence, Reynolds number must be higher than 2,000 theoretically, but it was only 0.003 for the flow in our microfluidic system, indicating laminar flow in this flow chamber system (Figure S2D). These results suggest that laminar flow with the presence of only shear stress and vorticity cannot induce highly efficient thrombopoiesis, but turbulent flow with an optimal level of shear stress and turbulent energy can.

Among the thrombopoietic chemical mediators identified (Figure 5), CCL5 (RANTES) is reportedly produced from platelets and promotes the formation of mouse proplatelets *in vitro* (Machlus et al., 2016; Tamura et al., 2016), but we found its influence was not dominant in our human cell system (Figure 5D; Video S7). The largest effects came from IGFBP2, MIF, and NRDC, none of which were previously reported to be involved in thrombopoiesis (Figures 5D and 5E; Video S7). Considering that these factors promoted platelet production in our shear-stress incorporated microfluidic system but not with turbulent flow, turbulence per se might be key for their release from imMKCLs. If true, it could be possible to improve other 3D flow chambers that have had good platelet yield by incorporating turbulent flow (Thon et al., 2014; Martinez et al., 2017). Turbulence may also explain how other organs besides the BM, such as the lung and spleen, may release platelets (Lefrançais et al., 2017).

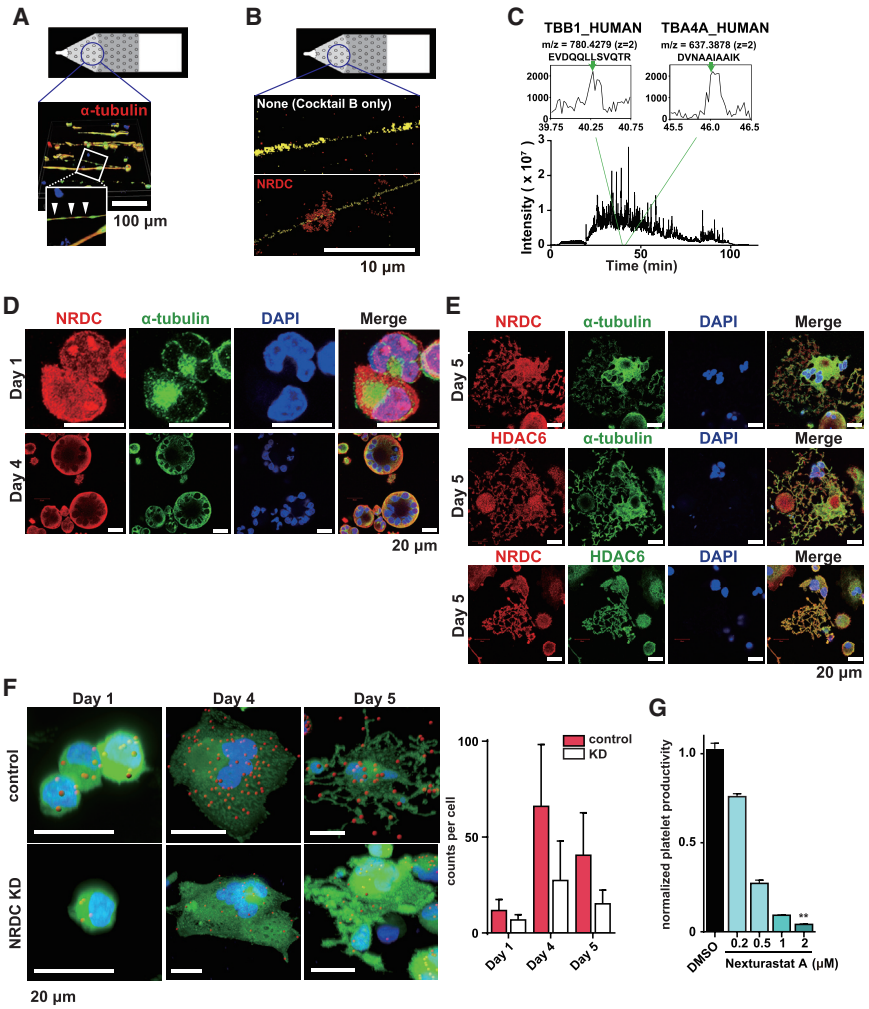

Figure 6. NRDC Contributes to Platelet Production in Extracellular Space and Intracellular Compartment

(A) Immunohistochemical images of proplatelets (red, α-tubulin; green, GFP) from imMKCLs in the microfluidic system (×400). Arrowheads: putative shedding sites. Scale bar, 100 μm.

(B) Super-resolution microscopic STORM analysis images of extracellular NRDC (red) around proplatelets (yellow, β1 tubulin) of imMKCLs in the microfluidic system (×1,000). Scale bar, 10 μm.

(C) IP-MS analysis against endogenous NRDC shows the specific binding of NRDC with α4A tubulin and β1 tubulin.

(D and E) Confocal micrographs of imMKCLs spread on days 1 and 4 (D), and day 5 (E) (×630). NRDC, α-tubulin, HDAC6, and DAPI. Scale bars, 20 μm.

(F) Duolink PLA analysis for control or active miRNA construct-treated imMKCLs (×600). Red, PLA signal for NRDC-HDAC6 foci; green, GFP; blue, DAP1. Scale bar, 20 μm. Right: mean dot number of NRDC-HDAC6 foci per cell. n = 4–16 cells.

(G) Dox-OFF stage imMKCLs were cultured for 6 days in the presence of cocktail B in a flask. Platelet yield was evaluated under the addition of DMSO or various concentrations of the HDAC6 inhibitor Nexturastat A. The number of $CD41a^+$ $CD42b^+$platelets in DMSO condition was set to 1.0. n = 3 experiments. **p < 0.01.

All data in (F) and (G) are means ± SD.

See also Figure S6.

Figure 7 depicts a proposed mechanism through which MIF, IGFBP2, and NRDC promote proplatelet shedding in the VerMES bioreactor. In the microfluidic system, MIF and IGFBP2 enhance the anchoring of megakaryocytes to pillars, which accelerates the formation of proplatelets possibly through the induction of ECM release. Although these pillars do not exist in the VerMES reactor, we speculate that ECM may mediate the formation of small megakaryocyte aggregates, thereby enhancing proplatelet formation.

Secreted NRDC may adhere to fragile points on proplatelets (Figure 6B), facilitating shear stress-induced platelet shedding through its peptidase activity (Figure 5D). On the other hand, our data suggest intracellular NRDC directly binds to tubulins (α4A-tubulin or β1-tubulin) (Figure 6C) and perhaps plays a role in tubulin conformation and remodeling by coordinating with HDAC6 (Figures 6E and 6F) (Hubbert et al., 2002; Miyake et al., 2016). A recent clinical trial for myeloma using a combination of chemotherapy and HDAC6 inhibitor Ricolinostat found a correlation between thrombocytopenia and the dosage of Ricolinostat independent of chemotherapy dose (Vogl et al., 2017), suggesting HDAC6 is an indispensable factor in human platelet biogenesis. Additionally, another report showed HDAC6 is crucial for proplatelet formation in humans through the deacetylation of cortactin (Messaoudi et al., 2017). Further studies are needed to clarify the interactions between NRDC, HDAC6, and cortactin.

To conclude, this study shows the crucial role of turbulence in platelet biogenesis and identified not only shear stress, an already known regulator (Junt et al., 2007; Thon et al., 2014; Blin et al., 2016), but also turbulent energy as a key parameter. Using this information, we succeeded in achieving the *ex vivo* production of platelets at clinical scale (100 billion-order). Using multiple animal models, our study provides a proof-of-concept for the clinical application of imMKCL-derived platelets generated through this turbulent flow-based model. As a next step, we aim to use washed-type concentrates in clinical trials. The scalable design of VerMES and the identification of two determinant physical parameters raise the anticipation of further developing a mass-scale bioreactor that can generate platelets at a large number of concentrates in a single batch. The discovery of turbulent energy and several thrombopoietic chemical mediators provides a new physico-chemical mechanism and *ex vivo* production strategy for platelet biogenesis that should impact studies in hematopoiesis and transfusion medicine as clinical scale cell therapies for regenerative medicine.

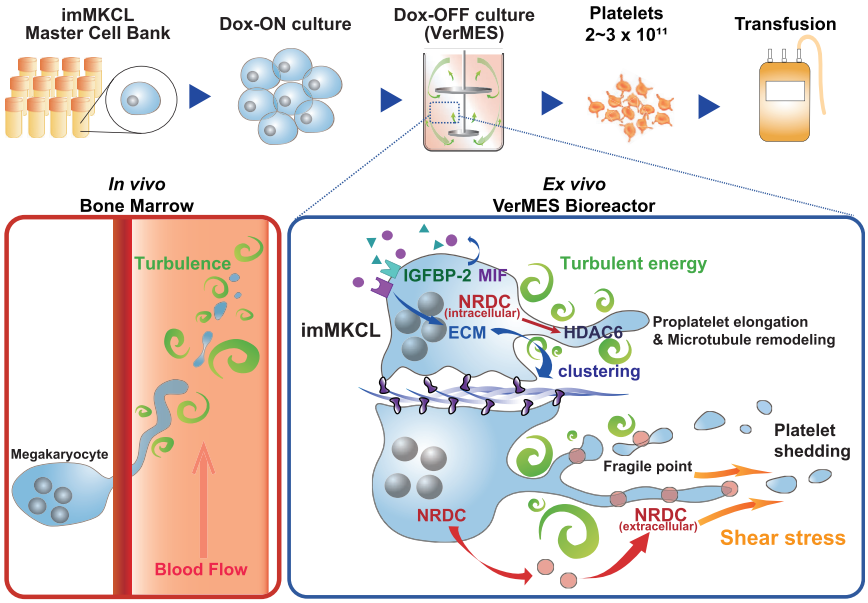

Figure 7. The Manufacturing of Washed-Type Platelet Concentrate from hiPSCs and a Hypothesized Cell-Autonomous Mechanism of Platelet Biogenesis

Dox-OFF stage imMKCLs in the presence of cocktail B release several factors, particularly IGFBP2, MIF, and NRDC, after stimulation with optimized shear stress and turbulent energy. Extracellular IGFBP2 and MIF promote the release of extracellular matrix (ECM) for cell clustering to support proplatelet elongation. NRDC mediates the shedding of proplatelets for platelet generation, which is promoted by shear stress. Simultaneously, endogenous (intracellular) NRDC collaborates with HDAC6 for proplatelet formation.

STAR★METHODS

Detailed methods are provided in the online version of this paper and include the following:

- KEY RESOURCES TABLE
- CONTACT FOR REAGENT AND RESOURCE SHARING
- EXPERIMENTAL MODEL AND SUBJECT DETAILS
  - Cell lines
  - Culture of imMKCLs
  - Platelet purification, washing and concentration
  - Animals
  - Human platelets
- METHOD DETAILS
  - Hemostatic and circulation tests with mice
  - Hemostatic and circulation tests with rabbits
  - *In vivo* analysis of thrombus formation
  - Flow cytometric analysis
  - Platelet Aggregation assay
  - Clot retraction assay
  - ELISA
  - Measurement of NRDC in culture medium
  - Platelet spreading assay
  - Electron microscopy
  - Microarray analysis
  - Protein array analysis
  - Quantitative RT-PCR
  - Immunofluorescence confocal microscopy
  - Intracellular staining flow cytometry
  - Super-resolution microscopy
  - Microfluidic system
  - DuoLink proximity ligation assay (PLA) analysis
  - VerMES bioreactors
  - Physical flow simulations in bioreactors
  - *In vivo* visualization of bone marrow megakaryocytes in eGFP transgenic mice and PIV analysis
  - Immunoprecipitation and liquid chromatography-mass spectrometry (LC-MS)
- QUANTIFICATION AND STATISTICAL ANALYSIS
  - Statistical Analysis
- DATA AND SOFTWARE AVAILABILITY

SUPPLEMENTAL INFORMATION

Supplemental Information includes six figures, one table, and seven videos and can be found with this article online at https://doi.org/10.1016/j.cell.2018.06.011.

ACKNOWLEDGMENTS

We thank Dr. P. Karagiannis for reading the manuscript, S. Akahane, Y. Kurokawa (Sanyo Chemical Industries, Ltd), C. Tokikura, M. Ueda, and M. Kawato for technical support, and Japanese Red Cross Society for providing donor-derived human platelets. This work was supported in part by Highway Program for Realization of Regenerative Medicine (JP17bm0504008 to K.E.), Practical Applications of Regenerative Medicine (JP17bk0104039 to K.E.), Core Center for iPS Cell Research (JP17bm0104001 to S.N., M.I., S.K., T.Y., N.S., and K.E.) from Japan Agency for Medical Research and Development (AMED), Grant-in-Aid for Scientific Research (15H03005 to K.E.)/Japan Society for the Promotion of Science (JSPS), and by Initiative for Accelerating Regulatory Science in Innovative Drug, Medical Device, and Regenerative Medicine/Ministry of Health, Labour and Welfare (MHLW) (to K.E.).

AUTHOR CONTRIBUTIONS

Conceptualization, Y.I., S. Nakamura, N.S., and K.E.; Formal Analysis, Y.I., S. Nakamura, Y.K., S.S., K.I., H.K., and T.Y.; Investigation, Y.I., S. Nakamura, S.S., K.I., H.K., T.S., H.H., H.O., K.F., T.M., N.H., K. Hashimoto, K. Harimoto, M. Nogawa, M.I., and S. Nishimura; Resources, Y.K., F.A., M.O., E.N., and K.E.; Writing – Original Draft, Y.I., S. Nakamura, N.S., and K.E.; Writing – Review & Editing, T.Y., E.N., N.W., F.A., S. Nishimura, N.S., and K.E.; Visualization, Y.I., S. Nakamura, S.K., A.S., and S. Nishimura; Supervision, M. Nakagawa, T.Y., E.N., N.W., M.H., F.A., S. Nishimura, and K.E.; Project Administration, K.E.; Funding Acquisition, K.E.

DECLARATION OF INTERESTS

Y.I., S. Nakamura, Y.K., and K.E. have applied for patents related to this manuscript. K.E. is a founder of Megakaryon Co. Ltd. The interests of K.E. were reviewed and are managed by Kyoto University in accordance with its conflict-of-interest policies.

Received: September 17, 2017
Revised: March 30, 2018
Accepted: May 23, 2018
Published: July 12, 2018

REFERENCES

Abbonante, V., Di Buduo, C.A., Gruppi, C., De Maria, C., Spedden, E., De Acutis, A., Staii, C., Raspanti, M., Vozzi, G., Kaplan, D.L., et al. (2017). A new path to platelet production through matrix sensing. Haematologica *102*, 1150–1160.

Aihara, A., Koike, T., Abe, N., Nakamura, S., Sawaguchi, A., Nakamura, T., Sugimoto, N., Nakauchi, H., Nishino, T., and Eto, K. (2017). Novel TPO receptor agonist TA-316 contributes to platelet biogenesis from human iPS cells. Blood Adv. *1*, 468–476.

Avanzi, M.P., Oluwadara, O.E., Cushing, M.M., Mitchell, M.L., Fischer, S., and Mitchell, W.B. (2016). A novel bioreactor and culture method drives high yields of platelets from stem cells. Transfusion *56*, 170–178.

Blin, A., Le Goff, A., Magniez, A., Poirault-Chassac, S., Teste, B., Sicot, G., Nguyen, K.A., Hamdi, F.S., Reyssat, M., and Baruch, D. (2016). Microfluidic model of the platelet-generating organ: beyond bone marrow biomimetics. Sci. Rep. *6*, 21700.

Coppé, J.P., Patil, C.K., Rodier, F., Sun, Y., Muñoz, D.P., Goldstein, J., Nelson, P.S., Desprez, P.Y., and Campisi, J. (2008). Senescence-associated secretory phenotypes reveal cell-nonautonomous functions of oncogenic RAS and the p53 tumor suppressor. PLoS Biol. *6*, 2853–2868.

Dempsey, G.T., Vaughan, J.C., Chen, K.H., Bates, M., and Zhuang, X. (2011). Evaluation of fluorophores for optimal performance in localization-based super-resolution imaging. Nat. Methods *8*, 1027–1036.

Di Buduo, C.A., Wray, L.S., Tozzi, L., Malara, A., Chen, Y., Ghezzi, C.E., Smoot, D., Sfara, C., Antonelli, A., Spedden, E., et al. (2015). Programmable 3D silk bone marrow niche for platelet generation ex vivo and modeling of megakaryopoiesis pathologies. Blood *125*, 2254–2264.

Dunois-Lardé, C., Capron, C., Fichelson, S., Bauer, T., Cramer-Bordé, E., and Baruch, D. (2009). Exposure of human megakaryocytes to high shear rates accelerates platelet production. Blood *114*, 1875–1883.

Gobbi, G., Mirandola, P., Carubbi, C., Masselli, E., Sykes, S.M., Ferraro, F., Nouvenne, A., Thon, J.N., Italiano, J.E., Jr., and Vitale, M. (2013). Proplatelet generation in the mouse requires PKCε-dependent RhoA inhibition. Blood *122*, 1305–1311.

Hahne, H., Pachl, F., Ruprecht, B., Maier, S.K., Klaeger, S., Helm, D., Médard, G., Wilm, M., Lemeer, S., and Kuster, B. (2013). DMSO enhances electrospray response, boosting sensitivity of proteomic experiments. Nat. Methods *10*, 989–991.

Hiraoka, Y., Yoshida, K., Ohno, M., Matsuoka, T., Kita, T., and Nishi, E. (2008). Ectodomain shedding of TNF-alpha is enhanced by nardilysin via activation of ADAM proteases. Biochem. Biophys. Res. Commun. *370*, 154–158.

Hirata, S., Murata, T., Suzuki, D., Nakamura, S., Jono-Ohnishi, R., Hirose, H., Sawaguchi, A., Nishimura, S., Sugimoto, N., and Eto, K. (2017). Selective inhibition of ADAM17 efficiently mediates glycoprotein Ibα retention during ex vivo generation of human induced pluripotent stem cell-derived platelets. Stem Cells Transl. Med. *6*, 720–730.

Hubbert, C., Guardiola, A., Shao, R., Kawaguchi, Y., Ito, A., Nixon, A., Yoshida, M., Wang, X.F., and Yao, T.P. (2002). HDAC6 is a microtubule-associated deacetylase. Nature *417*, 455–458.

Junt, T., Schulze, H., Chen, Z., Massberg, S., Goerge, T., Krueger, A., Wagner, D.D., Graf, T., Italiano, J.E., Jr., Shivdasani, R.A., and von Andrian, U.H. (2007). Dynamic visualization of thrombopoiesis within bone marrow. Science *317*, 1767–1770.

Kanda, K., Komekado, H., Sawabu, T., Ishizu, S., Nakanishi, Y., Nakatsuji, M., Akitake-Kawano, R., Ohno, M., Hiraoka, Y., Kawada, M., et al. (2012). Nardilysin and ADAM proteases promote gastric cancer cell growth by activating intrinsic cytokine signalling via enhanced ectodomain shedding of TNF-α. EMBO Mol. Med. *4*, 396–411.

Larson, M.K., and Watson, S.P. (2006). Regulation of proplatelet formation and platelet release by integrin alpha IIb beta3. Blood *108*, 1509–1514.

Lefrançais, E., Ortiz-Muñoz, G., Caudrillier, A., Mallavia, B., Liu, F., Sayah, D.M., Thornton, E.E., Headley, M.B., David, T., Coughlin, S.R., et al. (2017). The lung is a site of platelet biogenesis and a reservoir for haematopoietic progenitors. Nature *544*, 105–109.

Li, J., Chu, M., Wang, S., Chan, D., Qi, S., Wu, M., Zhou, Z., Li, J., Nishi, E., Qin, J., and Wong, J. (2012). Identification and characterization of nardilysin as a novel dimethyl H3K4-binding protein involved in transcriptional regulation. J. Biol. Chem. *287*, 10089–10098.

Lim, C.K., Hwang, W.Y., Aw, S.E., and Sun, L. (2008). Study of gene expression profile during cord blood-associated megakaryopoiesis. Eur. J. Haematol. *81*, 196–208.

Lupše, J., Škerget, L., and Ravnik, J. (2014). Velocity–vorticity RANS turbulence modeling by boundary element method. Eng. Anal. Bound. Elem. *39*, 44–52.

Machlus, K.R., Johnson, K.E., Kulenthirarajan, R., Forward, J.A., Tippy, M.D., Soussou, T.S., El-Husayni, S.H., Wu, S.K., Wang, S., Watnick, R.S., et al. (2016). CCL5 derived from platelets increases megakaryocyte proplatelet formation. Blood *127*, 921–926.

Madoiwa, S., Komatsu, N., Mimuro, J., Kimura, K., Matsuda, M., and Sakata, Y. (1999). Developmental expression of plasminogen activator inhibitor-1 associated with thrombopoietin-dependent megakaryocytic differentiation. Blood *94*, 475–482.

Martinez, A.F., McMahon, R.D., Horner, M., and Miller, W.M. (2017). A uniform-shear rate microfluidic bioreactor for real-time study of proplatelet formation and rapidly-released platelets. Biotechnol. Prog. *33*, 1614–1629.

Masuda, T., Sugiyama, N., Tomita, M., and Ishihama, Y. (2011). Microscale phosphoproteome analysis of 10,000 cells from human cancer cell lines. Anal. Chem. *83*, 7698–7703.

Messaoudi, K., Ali, A., Ishaq, R., Palazzo, A., Sliwa, D., Bluteau, O., Souquère, S., Muller, D., Diop, K.M., Rameau, P., et al. (2017). Critical role of the HDAC6-cortactin axis in human megakaryocyte maturation leading to a proplatelet-formation defect. Nat. Commun. *8*, 1786.

Miyake, Y., Keusch, J.J., Wang, L., Saito, M., Hess, D., Wang, X., Melancon, B.J., Helquist, P., Gut, H., and Matthias, P. (2016). Structural insights into HDAC6 tubulin deacetylation and its selective inhibition. Nat. Chem. Biol. *12*, 748–754.

Moreau, T., Evans, A.L., Vasquez, L., Tijssen, M.R., Yan, Y., Trotter, M.W., Howard, D., Colzani, M., Arumugam, M., Wu, W.H., et al. (2016). Large-scale production of megakaryocytes from human pluripotent stem cells by chemically defined forward programming. Nat. Commun. *7*, 11208.

Nakagawa, Y., Nakamura, S., Nakajima, M., Endo, H., Dohda, T., Takayama, N., Nakauchi, H., Arai, F., Fukuda, T., and Eto, K. (2013). Two differential flows in a bioreactor promoted platelet generation from human pluripotent stem cell-derived megakaryocytes. Exp. Hematol. *41*, 742–748.

Nakamura, S., Takayama, N., Hirata, S., Seo, H., Endo, H., Ochi, K., Fujita, K., Koike, T., Harimoto, K., Dohda, T., et al. (2014). Expandable megakaryocyte cell lines enable clinically applicable generation of platelets from human induced pluripotent stem cells. Cell Stem Cell *14*, 535–548.

Nesvizhskii, A.I., and Aebersold, R. (2005). Interpretation of shotgun proteomic data: the protein inference problem. Mol. Cell. Proteomics *4*, 1419–1440.

Nishi, E. (2013). Nardilysin. In Handbook of Proteolytic Enzymes, N. Rawlings and G. Salvesen, eds. (London: Academic Press), pp. 1421–1426.

Nishimura, S., Manabe, I., Nagasaki, M., Kakuta, S., Iwakura, Y., Takayama, N., Ooehara, J., Otsu, M., Kamiya, A., Petrich, B.G., et al. (2012). In vivo

imaging visualizes discoid platelet aggregations without endothelium disruption and implicates contribution of inflammatory cytokine and integrin signaling. Blood *119*, e45–e56.

Nishimura, S., Nagasaki, M., Kunishima, S., Sawaguchi, A., Sakata, A., Sakaguchi, H., Ohmori, T., Manabe, I., Italiano, J.E., Jr., Ryu, T., et al. (2015). IL-1α induces thrombopoiesis through megakaryocyte rupture in response to acute platelet needs. J. Cell Biol. *209*, 453–466.

Ohta, S., Nishida, E., Yamanaka, S., and Yamamoto, T. (2013). Global splicing pattern reversion during somatic cell reprogramming. Cell Rep. *5*, 357–366.

Oikawa, S., Sasaki, D., Kikuchi, M., Sawamura, Y., and Itoh, T. (2013). Comparative in vitro evaluation of apheresis platelets stored with 100% plasma versus bicarbonated Ringer's solution with less than 5% plasma. Transfusion *53*, 655–660.

Okuda, S., Watanabe, Y., Moriya, Y., Kawano, S., Yamamoto, T., Matsumoto, M., Takami, T., Kobayashi, D., Araki, N., Yoshizawa, A.C., et al. (2017). jPOSTrepo: an international standard data repository for proteomes. Nucleic Acids Res. *45* (D1), D1107–D1111.

Pallotta, I., Lovett, M., Rice, W., Kaplan, D.L., and Balduini, A. (2009). Bone marrow osteoblastic niche: a new model to study physiological regulation of megakaryopoiesis. PLoS ONE *4*, e8359.

Poirault-Chassac, S., Nguyen, K.A., Pietrzyk, A., Casari, C., Veyradier, A., Denis, C.V., and Baruch, D. (2013). Terminal platelet production is regulated by von Willebrand factor. PLoS ONE *8*, e63810.

Sim, X., Poncz, M., Gadue, P., and French, D.L. (2016). Understanding platelet generation from megakaryocytes: implications for in vitro-derived platelets. Blood *127*, 1227–1233.

Strassel, C., Eckly, A., Léon, C., Petitjean, C., Freund, M., Cazenave, J.P., Gachet, C., and Lanza, F. (2009). Intrinsic impaired proplatelet formation and microtubule coil assembly of megakaryocytes in a mouse model of Bernard-Soulier syndrome. Haematologica *94*, 800–810.

Strassel, C., Brouard, N., Mallo, L., Receveur, N., Mangin, P., Eckly, A., Bieche, I., Tarte, K., Gachet, C., and Lanza, F. (2016). Aryl hydrocarbon receptor-dependent enrichment of a megakaryocytic precursor with a high potential to produce proplatelets. Blood *127*, 2231–2240.

Stroncek, D.F., and Rebulla, P. (2007). Platelet transfusions. Lancet *370*, 427–438.

Strüßmann, T., Tillmann, S., Wirtz, T., Bucala, R., von Hundelshausen, P., and Bernhagen, J. (2013). Platelets are a previously unrecognised source of MIF. Thromb. Haemost. *110*, 1004–1013.

Takayama, N., Nishimura, S., Nakamura, S., Shimizu, T., Ohnishi, R., Endo, H., Yamaguchi, T., Otsu, M., Nishimura, K., Nakanishi, M., et al. (2010). Transient activation of c-MYC expression is critical for efficient platelet generation from human induced pluripotent stem cells. J. Exp. Med. *207*, 2817–2830.

Takizawa, H., Eto, K., Yoshikawa, A., Nakauchi, H., Takatsu, K., and Takaki, S. (2008). Growth and maturation of megakaryocytes is regulated by Lnk/Sh2b3 adaptor protein through crosstalk between cytokine- and integrin-mediated signals. Exp. Hematol. *36*, 897–906.

Takizawa, H., Nishimura, S., Takayama, N., Oda, A., Nishikii, H., Morita, Y., Kakinuma, S., Yamazaki, S., Okamura, S., Tamura, N., et al. (2010). Lnk regulates integrin alphaIIbbeta3 outside-in signaling in mouse platelets, leading to stabilization of thrombus development in vivo. J. Clin. Invest. *120*, 179–190.

Tamura, S., Suzuki-Inoue, K., Tsukiji, N., Shirai, T., Sasaki, T., Osada, M., Satoh, K., and Ozaki, Y. (2016). Podoplanin-positive periarteriolar stromal cells promote megakaryocyte growth and proplatelet formation in mice by CLEC-2. Blood *127*, 1701–1710.

Thon, J.N., Montalvo, A., Patel-Hett, S., Devine, M.T., Richardson, J.L., Ehrlicher, A., Larson, M.K., Hoffmeister, K., Hartwig, J.H., and Italiano, J.E., Jr. (2010). Cytoskeletal mechanics of proplatelet maturation and platelet release. J. Cell Biol. *191*, 861–874.

Thon, J.N., Mazutis, L., Wu, S., Sylman, J.L., Ehrlicher, A., Machlus, K.R., Feng, Q., Lu, S., Lanza, R., Neeves, K.B., et al. (2014). Platelet bioreactor-on-a-chip. Blood *124*, 1857–1867.

Vogl, D.T., Raje, N., Jagannath, S., Richardson, P., Hari, P., Orlowski, R., Supko, J.G., Tamang, D., Yang, M., Jones, S.S., et al. (2017). Ricolinostat, the first selective histone deacetylase 6 inhibitor, in combination with bortezomib and dexamethasone for relapsed or refractory multiple myeloma. Clin. Cancer Res. *23*, 3307–3315.

Wallace, J.M., and Foss, J.F. (1995). The measurement of vorticity in turbulent flows. Annu. Rev. Fluid Mech. *27*, 469–514.

Watanabe, N., Nogawa, M., Ishiguro, M., Maruyama, H., Shiba, M., Satake, M., Eto, K., and Handa, M. (2017). Refined methods to evaluate the in vivo hemostatic function and viability of transfused human platelets in rabbit models. Transfusion *57*, 2035–2044.

Whitaker, B.I., and Hinkins, S. (2011). The 2011 National Blood Collection and Utilization Survey Report (Washington, DC, USA: The United States Department of Health and Human Services).

Yamana, R., Iwasaki, M., Wakabayashi, M., Nakagawa, M., Yamanaka, S., and Ishihama, Y. (2013). Rapid and deep profiling of human induced pluripotent stem cell proteome by one-shot NanoLC-MS/MS analysis with meter-scale monolithic silica columns. J. Proteome Res. *12*, 214–221.

Zhang, Y., Conti, M.A., Malide, D., Dong, F., Wang, A., Shmist, Y.A., Liu, C., Zerfas, P., Daniels, M.P., Chan, C.C., et al. (2012). Mouse models of MYH9-related disease: mutations in nonmuscle myosin II-A. Blood *119*, 238–250.

STAR★METHODS

KEY RESOURCES TABLE

REAGENT or RESOURCE	SOURCE	IDENTIFIER
Antibodies		
Alexa Flour ™ 568 Phalloidin	Thermo	Cat#12380
anti-hCD41-APC	Biolegend Inc	Cat#303710; RRID: AB_2249385
anti-hCD42b-PE	Biolegend Inc	Cat#303906; RRID: AB_314386
anti-hCD235ab-PB	Biolegend Inc	Cat#306612; RRID: AB_2116241
anti-hCD62P-APC	Biolegend Inc	Cat#304910; RRID: AB_314482
anti-hCD42a-eFluoro 450 antibody	eBioscience	Cat#48-0428-42; RRID: AB_10805521
anti-hCD42a-PE	BD	Cat#558819; RRID: AB_397130
anti-hCD49b-PE	BD	Cat#555669; RRID: AB_396022
anti-hCD29-PE	BD	Cat#555443; RRID: AB_395836
anti-hCD32a-FITC	STEMCELL Technologies	Cat#60012FI; RRID: AB_2722545
anti-hGPVI-PE	Nakamura et al., 2014	N/A
FITC-PAC-1 antibodies	BD	Cat#340507; RRID: AB_2230769
FITC Annexin V antibodies	BD	Cat#556419; RRID: AB_2665412
rabbit anti–β1-tubulin antibodies	MBL	Cat#PD033; RRID: AB_10598497
mouse anti–α-tubulin antibodies	Sigma Aldrich	Cat#T5186
rabbit anti–α-tubulin antibodies	Abcam	Cat#ab52866; RRID: AB_869989
rabbit anti-HDAC6 antibodies	CST	Cat#7612; RRID: AB_10889735
mouse anti-NRDC antibodies	Kanda et al., 2012	N/A
Alexa Fluor 488 goat anti-mouse secondary antibodies	Thermo	Cat#A11001; RRID: AB_2534069
Alexa Fluor 488 goat anti-rabbit secondary antibodies	Thermo	Cat#A11008; RRID: AB_143165
Alexa Fluor 555 goat anti-mouse secondary antibodies	Thermo	Cat#A21422; RRID: AB_2535844
Alexa Fluor 555 goat anti-rabbit secondary antibodies	Thermo	Cat#A21428; RRID: AB_2535849
Zombie NIR	Bio Legend	Cat#423105
mouse anti-fibrinogen antibodies	Abcam	Cat#ab134047; RRID: AB_444752
mouse anti-fibronectin antibodies	Novus	Cat#NBP2-22113
mouse anti-von Willebrand factor antibodies	Abcam	Cat#ab194405
rabbit anti-vascular cell adhesion molecule-1 antibodies	Abcam	Cat#ab134047; RRID: AB_2721053
rabbit anti-collagen type IV alpha 2 chain antibodies	ABGENT	Cat#AP11454a; RRID: AB_10819194
rabbit anti-vitronectin antibodies	LS Bio	Cat#LS-C160558
Alexa Fluor 647-goat anti-mouse secondary antibodies	Thermo	Cat#A-21235; RRID: AB_2535804
Anti-human NRDC clone#231	This paper	N/A
Anti-human NRDC clone#304	This paper	N/A
Chemicals, Peptides, and Recombinant Proteins		
SR-1, AhR antagonist	Merck Millipore	Cat#182706
HIF Prolyl Hydroxylase Inhibitor	Merck Millipore	Cat#400084
JNJ-42041935, HIF-PHD inhibitor 2	Merck Millipore	Cat#400093
Y-27632, ROCK inhibitor	WAKO	Cat#400084
DAPT, P2Y12 inhibitor	WAKO	Cat#045-30981
Ac-DEVD-CHO, caspase 3 inhibitor	CAYMAN	Cat#10017
CAY10566, SCD1 inhibitor	CAYMAN	Cat#10012562
XAV939, tankyrase specific inhibitor	CAYMAN	Cat#13596
IOX2, PHD inhibitor	Axon Medchem	Cat#Axon1921

(*Continued on next page*)

Continued

REAGENT or RESOURCE	SOURCE	IDENTIFIER
SB431542, TGF-beta receptor 1 kinase inhibitor	Axon Medchem	Cat#Axon1661
PRT4165, Bmi-Ring1A E3 ligase inhibitor	Axon Medchem	Cat#Axon1953
LY294002, PI3K inhibitor	Axon Medchem	Cat#Axon1366
CHIR99021, GSK-3 inhibitor	Axon Medchem	Cat#Axon1386
S1P, sphingosine-1-phosphate	TOCRIS	Cat#1370
Z-VAD-FMK, pan caspase inhibitor	TOCRIS	Cat#2163
Rapamycin, Ser/Thr protein kinase mTOR inhibitor	TOCRIS	Cat#1292
DMH1, BMP inhibitor 2	TOCRIS	Cat#4126
RP001, S1P1 specific agonist	TOCRIS	Cat#4289
CYM5442, high selective S1P1 agonist	TOCRIS	Cat#3601
JTE013, S1P2 receptor antagonist	TOCRIS	Cat#2392
SPG, Schizophyllan	Invivogen	Cat#tlrl-spg
W146, S1P1 antagonist	Avanti Polar Lipids	Cat#857390
Nexturastat A, HDAC6 inhibitor	Adipogen lifescience	Cat#AG-CR1-3901
recombinant human (rh) Thrombospondin-1	R&D Systems	Cat#3074-TH
rhCCL5	R&D Systems	Cat#278-RN
rhPAI-1	R&D Systems	Cat#1786-PI
rhIGFBP-2	R&D Systems	Cat#674-B2
rhMIF	R&D Systems	Cat#289-MF
rhNRDC	Sysmex	N/A
rhNRDC_E > A	Sysmex	N/A
animal-derived-free recombinant human stem cell factor	Wako	Cat#193-15513
TA-316	Nissan Chemical	N/A
human serum	Cosmo Bio	Cat#12181201
human plasma	Cosmo Bio	Cat#12250210
human plasma	Japan blood products organization	N/A
Heparin sodium	Yoshido Inc.	Cat#(01)14987476163428
KP-457	Kaken Pharmaceutical	N/A
GNF-351	Calbiochem	Cat#182707
Y39983	MedChemExpress	Cat#HY-10069
PMA	Sigma Aldrich	Cat#P1585
TRAP-6	BACHEM	Cat#H-8365.0005
ADP	Sigma Aldrich	Cat#A-2754
Complete mini	Roche Applied Science	Cat#04693159001
Dynabeads protein G	VERITAS	Cat#DB10009
BS3 (bis(sulfosuccinimidyl)suberate)	Thermo	Cat#21580
Hoechst 33342	Thermo	Cat#H1399
Texas Red-dextran	Thermo	Cat#D1830
Critical Commercial Assays		
miRNeasy Mini Kit	QIAGEN	Cat#217004
ReverTra Ace® qPCR RT Master Mix with gDNA Remover	TOYOBO	Cat#FSQ-301
EagleTaq Universal Master Mix (ROX)	Roche Applied Science	Cat#07260288190
Universal ProbeLibrary Set, Human	Roche Applied Science	Cat#04683633001
PF4 TMB ELISA kit	Roche Diagnostics	Cat#630430
beta TG TMB ELISA kit	Roche Diagnostics	Cat#630232
Proteome Profiler Human XL Cytokine Array Kit	R&D systems	Cat#ARY022
GeneChip Human Gene 2.0 ST Aassy	Thermo	Cat#902458

(*Continued on next page*)

Continued

REAGENT or RESOURCE	SOURCE	IDENTIFIER
GeneChip WT PLUS Reagent Kit	Thermo	Cat#902280
PerFix-nc	Beckman Coulter	Cat#B31167
Duolink *In Situ* PLA Probe Anti-Rabbit PLUS	Sigma-Aldrich	Cat#DUO92002
Duolink *In Situ* PLA Probe Anti-Mouse MINUS	Sigma-Aldrich	Cat#DUO92004
Duolink *In Situ* Detection Reagents Red	Sigma-Aldrich	Cat#DUO92008
Duolink *In Situ* Mounting Medium with DAP1	Sigma-Aldrich	Cat#DUO82040
Duolink *In Situ* Wash Buffer, Fluorescence	Sigma-Aldrich	Cat#DUO82049
iTRAQ Reagents Multiplex Kit	Sciex	Cat#4352135
BD TrucountTM Tubes	BD	Cat#340334
Flow Cytometry Size Calibration Kit	Thermo	Cat#F13838
Lenti-X^{TM} qRT-PCR Titration Kit	Clontech	Cat#631235
Deposited Data		
MS/MS data	This paper	PXD009739 (JPST000418)
Microarray data	This paper	GSE112512
Oligonucleotides		
Primers for RTqPCR assay, see Table S1	This paper	N/A
Experimental Models: Cell Lines		
imMKCL clone 7	Nakamura et al., 2014	N/A
imMKCL clone N5-6	This paper	N/A
imMKCL clone MK04	This paper	N/A
Experimental Models: Organisms/Strains		
NOG (NOD.Cg-*Prkdc*^{scid}*Il2rg*^{tm1Sug}/ShiJic) mice	the Central Institute for Experimental Animals	https://www.invivoscience.com/en/index.html
New Zealand white rabbits	Watanabe et al., 2017	N/A
CAG-eGFP C57BL/6 strain mice	Nishimura et al., 2015	N/A
Software and Algorithms		
GeneSpring GX software	Agilent Technologies	https://www.agilent.com/en/products/software-informatics/life-sciences-informatics/genespring-gx
NIS-Elements software	Nikon	https://www.nikon.com/products/microscope-solutions/lineup/img_soft/nis-elements/
Image Quant TL	GE healthcare	https://www.gelifesciences.co.jp/catalog/1167.html
COMSOL Multiphysics v 5.2	COMSOL AB	https://www.comsol.com/release/5.2
Imaris	BITPLANE	http://www.bitplane.com/
FlowExpert2D2C	Kato Koken	http://www.kk-co.jp/products/flow2d2c.php
Mascot Server v2.5	Matrix Science	http://www.matrixscience.com/
ProteinPilot v5.0	Sciex	https://sciex.com/products/software/proteinpilot-software
Graph pad Prism 6	Graph Pad software	https://www.graphpad.com/scientific-software/prism/
FlowJo	FlowJo, LLC	https://www.flowjo.com/solutions/flowjo

CONTACT FOR REAGENT AND RESOURCE SHARING

Further information and requests for resources and reagents should be directed to and will be fulfilled by the Lead Contact, Koji Eto (kojieto@cira.kyoto-u.ac.jp)

EXPERIMENTAL MODEL AND SUBJECT DETAILS

Cell lines

The three imMKCL clones (CL-7, N5-6, and MK04) were each established from different iPSC clones. iPSC clones were derived from Caucasian male newborn fibroblast, male newborn cord blood $CD34^+$ cells of unknown ethnicity and Asian female peripheral blood T cells for CL-7, N5-6, and MK04, respectively. Lentiviral particles in culture media were confirmed negative by using Lenti-X™ qPCR titration kit (Clontech). All imMKCLs were established using mitomycin C-treated mouse C3H10T1/2 cells as previously described (Nakamura et al., 2014). The mouse C3H10T1/2 feeder cell line was from the Riken Bio-Resource Center (Tsukuba, Ibaraki, Japan). For GMP grade assurance of N5-6 and MK04 imMKCLs, we validated the GMP grade screening of C3H10T1/2 cells by a certified testing service company to rule out viral contamination in the final products. Other products for the imMKCL generation were also of GMP grade.

Culture of imMKCLs

Dox-ON proliferation culture

imMKCLs were cultured in the presence of doxycycline to proliferate by the expression of three doxycycline-regulated transgenes: c-MYC, BMI1, and BCL-XL (Nakamura et al., 2014). imMKCLs were cultured in a humidified incubator at 37°C and 5% CO_2 and passaged to maintain 1×10^5 ~2×10^6 cells/mL in basal medium supplemented with 15% fetal bovine serum (FBS; 172012; Sigma-Aldrich) and cocktail A. FBS was pre-treated with 35 kGy irradiation. Basal medium consisted of IMDM (Sigma-Aldrich #I3390) supplemented with L-glutamine (25030-081; Thermo Fisher Scientific), Insulin-transferrin-selenium (41400-045; Thermo), 50 μg/mL Ascorbic acid (A4544; Sigma-Aldrich), and 450 μM 1-Thioglycerol (M6145; Sigma-Aldrich). Cocktail A consisted of 50 ng/mL animal-derived-free recombinant human stem cell factor (SCF; 193-15513; Wako), 200 ng/mL TA-316 (Nissan Chemical), and 5 μg/mL Doxycycline (631311; Clontech).

Dox-OFF differentiation culture

Culture for imMKCL maturation was done in a humidified incubator at 37°C and 5% CO_2 with 1×10^5 or 2×10^5 cells/mL for 6~7 days in basal medium supplemented with cocktail B and serum or plasma. The following were used as serum or plasma: 15% FBS or various concentrations of human plasma (Cosmo Bio #12250210, Japan blood products organization) or human serum (Cosmo Bio #12181201). 10 U Heparin sodium (Yoshido Inc. #(01)14987476163428) was added in the case of human plasma. Cocktail B consisted of 50 ng/mL SCF, 200 ng/mL TA-316, 15 μM KP-457 (Kaken Pharmaceutical), 0.75 μM SR-1 (Calbiochem) or 0.5 μM GNF-351 (Calbiochem), and 10 μM Y27632 (Wako) or 0.5 μM Y39983 (MedChemExpress). Dox-OFF stage imMKCLs were cultured in 125, 250, or 500 mL Corning® Erlenmeyer cell culture flasks (#431143, #431144 and #431145; Sigma-Aldrich) in shaking conditions using Lab-Therm shaker (Kuhner). Dox-OFF stage imMKCL culture in the reactor was done using VerMES (SATAKE Co,.Ltd., Saitama, Japan).

Platelet purification, washing and concentration

After 6 days of maturing the imMKCLs, platelet-containing culture suspensions were subject to hollow fiber filtration to reduce the volume, followed by washing and depletion of the remaining imMKCLs using the ACP centrifugation system (HAEMONETICS ACP®215). Platelets were re-suspended in platelets storage solution consisting of bicarbonated Ringer's solution with ACD-A solution (5%–20%) plus 2.5% albumin (Oikawa et al., 2013).

Animals

Animals were group housed on a 12 h light/12 h dark cycle with *ad libitum* access to food and water under specific pathogen free conditions in individually ventilated cages. NOG (NOD.Cg-*Prkdc*^{scid}*Il2rg*^{tm1Sug}/ShiJic) mice were purchased from the Central Institute for Experimental Animals (Kawasaki, Kanagawa, Japan). Male, 14–16 weeks old, New Zealand white rabbits (body weight 2.5~3.0 kg) were used for this study in accordance with a protocol approved by the Laboratory Animal Center of Keio University School of Medicine. All animal experiments at Kyoto University conformed to ethical principles and guidelines approved by the Ethical Committee of Kyoto University. CAG-eGFP C57BL/6 strain mice were used for *in vivo* thrombopoiesis visualization as described previously (Nishimura et al., 2015). All animal experiments at Jichi Medical University conformed to ethical principles and guidelines approved by the Ethical Committee of Jichi Medical University.

Human platelets

Donor-derived human platelets were provided from the Japanese Red Cross Society. Human platelets and plasma were used in compliance with the Guidelines on the use of Donated blood in R&D, etc. from Ministry of Health, Labour and Welfare of Japan.

METHOD DETAILS

Hemostatic and circulation tests with mice

As previously reported (Takizawa et al., 2010), thrombocytopenia was induced by 2.4 Gy gamma irradiation to 10-12-wk-old male NOG mice. Nine days after irradiation, mice were infused with 2×10^8 platelets (100 μL of 2×10^9 platelets/mL) or vehicle to the

tail vein under anesthesia. Then, hemostasis was assessed by tail bleeding, which was caused by puncture with a 23G needle to the tail artery 2 cm from the tip. In the circulating model, peripheral blood sampling was done from the external jugular vein before and 0.5, 1, 2, 4, 6, 24, 48 h after infusion, and the ratio of infused human platelets was analyzed by flow cytometric analysis.

Hemostatic and circulation tests with rabbits

Experiments were done according to a recent report (Watanabe et al., 2017). Thrombocytopenia was induced by the intraperitoneal administration of busulfan at two time points (18.75 mg/kg on day 1 and 23.25 mg/mL on day 3) to rabbits. At days 14-16, blood platelet counts of the busulfan-treated rabbits had decreased to less than $2.5 \times 10^4/\mu L$. To block the reticuloendothelial system and inhibit the rapid clearance of infused platelets due to xenografting, 0.75 mg/kg of emulsified ethylpalmitate (EP) was administrated into the marginal ear vein at 1 day before platelet infusion. Then, 1×10^{10} platelets/2.5 kg body weight were injected into the right ear marginal vein at 1 mL/min using a syringe pump under anesthesia. The bleeding times were measured at two sites of the left ear marginal vein wounded by Quikheel Lancet (depth 1 mm, width 2.5 mm). In this hemostatic model, bleeding times of more than 600 s were defined as non-hemostatic. In the circulation model, splenectomy was done 2 weeks before, and EP was administrated 1 day before platelet infusion. Blood sampling was done from the ear marginal vein at 10 min, 20 min, and 1, 2.5, 4, 23 h after infusion.

In vivo analysis of thrombus formation

NOG mice were initially irradiated (2.4 Gy) to induce thrombocytopenia 9 days before transfusion, after which they were used for *in vivo* imaging studies. *In vivo* analysis of thrombus formation was performed as described previously (Nakamura et al., 2014; Nishimura et al., 2012). In brief, we performed *in vivo* laser- and reactive-oxygen-species-induced injury, and images were acquired using a resonance-scanning confocal microscope (Nikon A1R System). The collected images were analyzed by observers blinded to the protocol using NIS-Elements software (Nikon).

Flow cytometric analysis

Flow cytometric analysis was performed by using FACSVerse and described previously (Nakamura et al. CSC). The following antibodies were used: anti-hCD41-APC (#303710), anti-hCD42b-PE (#303906), anti-hCD235ab-PB (#306612), and anti-hCD62P-APC (#304910) antibodies obtained from Biolegend Inc.; anti-hCD42a-eFluoro 450 antibody from eBioscience (#48-0428-42); FITC-PAC-1 (#340507), FITC Annexin V (#556419), anti-hCD42a-PE (#558819), anti-hCD49b-PE (#555669), and anti-hCD29-PE (#555443) antibodies from BD; and anti-hCD32a-FITC (60012FI) antibody from STEMCELL Technologies; anti-hGPVI-PE antibody was kindly provided by Dr. C. Ghevaert, (University of Cambridge, UK). Before and after activation by 40 μM TRAP-6 (BACHEM #H-8365.0005) and 100 μM ADP (Sigma Aldrich #A-2754) or 20 μM ionomycin (Wako #091-05833), platelets were measured for the staining of PAC1, CD62P and Annexin V.

Platelet Aggregation assay

Platelet aggregation was analyzed by an aggregation analyzer (Kowa PA-200C). Stored human donor platelets or iPSC-platelets were prepared for washed platelets and re-suspended in 70% human plasma (3×10^8 platelets/mL) with 3 mM $CaCl_2$. 270 μL of the sample preparation was mixed with 30 μL of stimuli solution including 5 μg/mL collagen and 10 μM ADP for 8 min at 37°C.

Clot retraction assay

Assays were carried out as previously reported (Takizawa et al., 2010). In brief, stored human donor platelets or iPSC-platelets suspended in 70% human plasma (3×10^8 cells/mL) with 3 mM $CaCl_2$ in the presence or absence of 10 U/mL thrombin were incubated at 37°C for 1 h to induce clot formation and retraction. After incubation, clots were removed, and the weight of the tubes without clots was measured. The ratio of clot retraction was calculated by the weight difference between the sample without platelets and the sample with platelets (the sample without platelets was set as 100%).

ELISA

For platelet factor 4 (PF4) and beta-thromboglobulin (βTG), 1.5×10^7 of donated platelets or iPSC-platelets were suspended in 500 μL of Tyrode's buffer and stimulated with 0.2 μM of PMA or 5, 10, 20, 40 μM of TRAP-6 at 25°C. Twenty minutes after platelet activation, supernatant was harvested with centrifugation at 2000 x g for 15 min. The released PF4 and βTG were measured using PF4 TMB ELISA kit (Roche Diagnostics #630430) and beta TG TMB ELISA kit (Roche Diagnostics #630232), respectively.

Measurement of NRDC in culture medium

NRDC in culture medium was quantified by chemiluminescent enzyme immunoassay as described (Kanda et al., 2012). The selected capture antibody (clone #231) against human recombinant NRDC (Met^{50}-Lys^{1150}) was conjugated to a glass bead, while the detection antibody (clone #304) was labeled with horseradish peroxidase (HRP). Culture medium was incubated with glass bead (#231), followed by incubation with #304 (5 μg/ml). The HRP activity of the immune complex was measured as the luminescent intensity using a fully automated system SphereLight 180 analyzer (Olympus, Tokyo, Japan). The values were compared to the luminescent intensity of known NRDC standards to determine the concentration of NRDC.

Platelet spreading assay

Assays were performed as described previously (Hirata et al., 2017; Takizawa et al., 2010). All observations were made using a confocal microscopic system (Zeiss LSM710; Oberkochen, Germany) equipped with a 63Å~/1.40 numeric aperture oil-immersion objective. imMKCL-derived platelets were attached on a fibrinogen (100 μg/ml)-coated cover glass. For activation, platelets were treated with 200 μM ADP and 40 μM TRAP-6. Then the cells were fixed, permeabilized, and stained with rhodamine-phalloidin (1:500; Thermo Fisher Scientific, Waltham, USA) to detect spreading F-actin fibers in activated platelets.

Electron microscopy

Dox-OFF stage imMKCL cells supplemented with or without SR1 and/or Y27632 or imMKCL-derived platelet pellets were fixed using a mixture of 0.5% glutaraldehyde and 2% paraformaldehyde in 0.1 M phosphate buffer (pH 7.4) for 60 min at 4°C. After washing with phosphate buffer, the samples were post-fixed with 1% osmium tetroxide in phosphate buffer for 60 min on ice. After dehydration, samples were infiltrated with and embedded in Epoxy resin. Ultrathin sections (60-80 nm thick) were cut and stained with 2% uranyl acetate in 70% methanol and with Reynolds' lead citrate and observed with a transmission electron microscope operating at 80 kV (HT-7700; Hitachi, Tokyo, Japan).

Microarray analysis

Total RNA was extracted using miRNeasy Mini Kit (QIAGEN, Valencia, CA, USA) according to the manufacturer's instructions. Microarray experiments were performed as described previously (Ohta et al., 2013) using the Affymetrix GeneChip Human Gene 2.0 ST array. Data analyses were performed using GeneSpring GX software (Agilent Technologies).

Protein array analysis

Proteome Profiler Human XL Cytokine Array Kit (R&D systems, Inc. #ARY022) was used. Culture supernatants were applied to the membranes included in the kit after filtration using a 0.22 μm filter (Merck Millipore). Data analyses were performed using Image Quant LAS 500 (GE healthcare). Sample intensities were normalized to positive control values included in each sample membrane and then compared between samples.

Quantitative RT-PCR

RNA was extracted using miRNeasy Mini Kit (QIAGEN, Valencia, CA, USA) according to the manufacturer's instructions. cDNAs were synthesized using ReverTra Ace® qPCR RT Master Mix with gDNA Remover (TOYOBO Osaka Japan). Real-time PCR was performed using EagleTaq Master Mix with ROX and Universal ProbeLibrary (Roche Applied Science, Penzberg, Germany) according to the manufacturer's instructions. Signals were detected using the ABI7900HT Real-Time PCR System (Applied Biosystems, Foster, CA). Primer sets for *GAPDH*, *IGFBP2*, *MIF*, *NRDC*, *TSP-1*, *CCL5*, and *PAI1* were determined using the Universal Probe Library Set for humans (https://qpcr.probefinder.com/input.jsp?organism=h_sap). Sequences of primers are listed in Table S1.

Immunofluorescence confocal microscopy

For immunofluorescence analyses, the cells were fixed in 4% paraformaldehyde (Wako) for 10 min and permeabilized with 0.1% Triton X-100 (Sigma) for 5 min. Thereafter, the specimens were blocked in 10% goat serum (Sigma) and incubated for 1 h with rabbit anti–β1-tubulin (MBL, Nagoya Japan), mouse anti–α-tubulin (Sigma), rabbit anti–α-tubulin (Abcam), rabbit anti-HDAC6 (CST), or mouse anti-NRDC (provided by E. Nishi (Kanda et al., 2012)) antibodies. They were then incubated for 0.5 h with Alexa Fluor 488 goat secondary antibodies against mouse or rabbit IgG (Thermo) and Alexa Fluor 555 goat secondary antibodies against mouse or rabbit IgG (Thermo). Finally, they were incubated in DAP1 (Vector), and images were captured using a confocal microscope (Zeiss LSM710) equipped with a 63 × /1.40 numeric aperture oil-immersion objective.

Intracellular staining flow cytometry

imMKCL cells at day 5 of the DOX-OFF stage after manipulation for 24 h were incubated with Zombie NIR(Bio Legend) for 30 min and then fixed and stained using PerFix-nc (Beckman Coulter) with the following antibodies: mouse anti-fibrinogen (Abcam), mouse anti-fibronectin (Novus), mouse anti-von Willebrand factor (vWF) (Abcam), rabbit anti-vascular cell adhesion molecule-1 (VCAM-1) (Abcam), rabbit anti-collagen type IV alpha 2 chain (COL4A2) (Abcam), and rabbit anti-vitronectin (LS Bio). The secondary antibodies used were Alexa Fluor 555-goat secondary antibodies against mouse or rabbit IgG (Thermo). The samples were analyzed using a FACSAria II instrument (BD Biosciences).

Super-resolution microscopy

STORM (stochastic optical reconstruction microscopy) analysis was performed based on previous reports (Dempsey et al., 2011). In brief, the cells were fixed in 4% paraformaldehyde (Wako) for 10 min and permeabilized with 0.1% Triton X-100 (Sigma) for 5 min. Thereafter, the specimens were blocked in 10% goat serum (Sigma) and incubated for 1 h with rabbit anti–β1-tubulin (MBL Aichi Japan) and mouse anti-NRDC (provided by E. Nishi) (Kanda et al., 2012) antibodies. They were then incubated for 0.5 h with Alexa

Fluor 555-goat anti-rabbit and Alexa Fluor 647-goat anti-mouse secondary antibodies (Thermo). Images were captured using a TIRF microscope (Nikon N-STORM System) equipped with SR Apo TIRF 100X 1.49 Oil. Super-resolution images were reconstructed after the acquisition of 30,000 images.

Microfluidic system

The microfluidic chip has a microchannel with a slope area where the ceiling gradually lowers to become 5 μm high and extends along a flat area at the 5 μm height (Figure S2C). The bottom part of the device is made of glass to enable microscopic observation. The microchannel contains pillars of 5 μm height and 10 μm diameter, each placed 20 μm apart. For platelet generation, (i) 1×10^4 imMKCLs expressing GFP from 5 days static culture in cocktail B were resuspended in 200 μL media and injected into the chip through the inlet. Then, 10 kPa was applied using a pneumatic pump for 0.5 h to trap the imMKCL in the narrowing slope area. (ii) Next, 1 mL medium was applied with 10 kPa, and excreted media from the outlet were analyzed after 1.5, 2.5, and 3.5 h. In this step, proplatelet formation and platelet production were observed by an IX73 microscope (Olympus, Tokyo, Japan). (iii) Finally, 1 mL of medium was applied with 100 kPa for 0.5 h to collect the produced platelets inside the microchannel. The flow conditions were analyzed using COMSOL Multiphysics v 5.2 (COMSOL AB, Stockholm, Sweden). Figure S2D shows the simulation results of velocity, shear rate and vorticity. In this simulation, the maximum shear rate was 2.1×10^3 s^{-1}.

The position of the analyzed portion of the microchannel was 2.5 μm above the bottom of the glass substrate.

DuoLink proximity ligation assay (PLA) analysis

Duolink® PLA (Sigma) was used to validate the association between HDAC6 and NRDC. imMKCLs were spread on a fibronectin-coated cover glass on days 1, 4 and 5, then fixed with 4% paraformaldehyde (Wako) for 10 min, permeabilized with 0.1% Triton X-100 (Sigma) for 5 min, blocked with 10% goat serum (Sigma), incubated for 1 h with rabbit anti-HDAC6 (CST) and mouse anti-NRDC (provided by E. Nishi) (Kanda et al., 2012) antibodies, incubated for 1 h with anti-mouse PLA MINUS and anti-rabbit PLA PLUS probes (Sigma), incubated for 0.5 h with a DNA ligase (Sigma), incubated for 100 min with DNA polymerase (Sigma), and incubated in DAPI (Sigma). Images were captured using a confocal microscope (Nikon A1R System) equipped with Plan Apo IR 60X 1.27 WI and reconstructed using Imaris image analysis software (Bitplane). NRDC-HDAC6 foci were counted in imMKCLs with ploidy of 2N or more on day 1, 4N or more on day 4 and in proplatelets on day 5.

VerMES bioreactors

VerMES reactors equipped with mixing blades moving vertically up and down were manufactured by Satake Co. Ltd. The operating conditions on a lab scale using a VerMES reactor were as follows. Setting velocity: 0 to 300 mm/s and stroke: up to 40 mm. A single blade was employed in a 500 mL tank containing 300 mL liquid volume, and two stage blades were employed in 3.0 L and 10.0 L tanks containing 2.4 L and 8.0 L liquid, respectively.

Optimal condition of the 8 L VerMES was as follows: stroke, 40 mm; speed 150 mm/s.

Physical flow simulations in bioreactors

Simulations were performed using CFD software that included the thermal fluid analysis module of Fluent 18 (ANSYS, Inc.). To ensure high accuracy of the simulation results, we conducted validations using *PTV* (Particle Tracking Method). For verification of the turbulence model, we performed the Realizable κ-ε model. Shear stress, strain rate, vorticity, turbulent energy, and energy dissipation were calculated using the equations shown below.

μ:viscosity coefficient
ν:kinematic viscosity
κ:turbulent energy
ε:energy dissipation
γ:shear rate
τ:shear stress
ω:vorticity

Turbulent energy, κ

$$\frac{\partial(\rho k)}{\partial t}+\frac{\partial\left(\rho\overline{U_i}k\right)}{\partial x_i}=\frac{\partial}{\partial x_i}\left\{\left(\mu+\frac{\mu_t}{\sigma_k}\right)\frac{\partial k}{\partial x_i}\right\}+P_k-\rho\varepsilon$$

$$\mu_t=C_\mu\rho\frac{k^2}{\varepsilon}$$

Energy dissipation of turbulence

$$\frac{\partial(\rho\varepsilon)}{\partial t}+\frac{\partial\left(\rho\overline{U_i}\varepsilon\right)}{\partial x_i}=\frac{\partial}{\partial x_i}\left\{\left(\mu+\frac{\mu_t}{\sigma_\varepsilon}\right)\frac{\partial\varepsilon}{\partial x_i}\right\}+\rho C_1 S_\varepsilon-\rho C_2\frac{\varepsilon^2}{k+\sqrt{\mu\varepsilon}}$$

Differencing method

Pressure	Second order central differencing
Momentum	Second order upwind differencing
Turbulent energy	Second order upwind differencing
Energy dissipation	Second order upwind differencing

Vector

$$v=(u,v,w)$$

Shear stress

$$\tau=\mu\dot{\gamma}$$

Strain rate

$$\dot{\gamma}=\sqrt{2\left[\left(\frac{\partial u}{\partial x}\right)^2+\left(\frac{\partial v}{\partial y}\right)^2+\left(\frac{\partial w}{\partial z}\right)^2\right]+\left(\frac{\partial u}{\partial y}+\frac{\partial v}{\partial x}\right)^2+\left(\frac{\partial v}{\partial z}+\frac{\partial w}{\partial y}\right)^2+\left(\frac{\partial w}{\partial x}+\frac{\partial u}{\partial z}\right)^2}$$

Vorticity

$$\omega=\|rot\ v\|$$
$$=\sqrt{\left(\frac{\partial w}{\partial y}-\frac{\partial v}{\partial z}\right)^2+\left(\frac{\partial u}{\partial z}-\frac{\partial w}{\partial x}\right)^2+\left(\frac{\partial v}{\partial x}-\frac{\partial u}{\partial y}\right)^2}$$

In vivo visualization of bone marrow megakaryocytes in eGFP transgenic mice and PIV analysis

Visualization was performed based on our original method (Nishimura et al., 2015). A two photon confocal microscope (Nikon A1R System) equipped with water immersion x40 lens (NA 1.15) was used to detect eGFP-expressing megakaryocytes in BM of the skull of living 5 week-old mice (CAG-eGFP C57BL/6 strain) under anesthesia (urethane, 1.5g/Kg) and secured to the heated piezo-drive stage (Tokai Hit; Nikon) of an inverted microscope (Eclipse Ti; Nikon). Texas Red-dextran (25 mg/kg BW) and Hoechst 33342 (10 mg/kg) were injected to visualize cell dynamics within BM of CAG-eGFP mice. After acquiring 30,000 sequential two-dimensional images at 120 frame per second (n = 5 mice, 10 different sites per each mouse), particle imaging velocimetry (PIV) analysis was done using FlowExpert2D2C software (Kato Koken, Kanagawa, Japan) (Wallace and Foss, 1995; Lupše et al., 2014). Movement velocity, vectors, and turbulence were visualized with pseudo color coding.

Immunoprecipitation and liquid chromatography-mass spectrometry (LC-MS)

5×10^6 megakaryocytes cultured in VerMES for 5 days were collected and homogenized in lysis buffer containing 10 mM Tris-HCL (PH7.4), 150 mM NaCl, 1% Nonidet P-40, and protease inhibitor mixture (Roche Applied Science). After sonication with Bioraptor, cell lysates were centrifuged at 13,000 rpm for 10 min and 4°C. The supernatant was incubated with rabbit monoclonal anti-mouse NRDC antibody (provided by E. Nishi) (Kanda et al., 2012), followed by the collection of immune complexes with magnetic beads in accordance with the manufacturer's instructions (Dynabeads:sigma) with some modifications. The magnetic beads were then washed with PBS and subsequently boiled in PTS buffer (100 mM Tris-HCl, 0.5% (w/v) sodium deoxycholate and 0.35% (w/v) sodium lauroyl sarcosinate, pH 9.0) (Masuda et al., 2011). Protein-containing supernatants were then collected.

Protein samples were subjected to reduction, alkylation, Lys-C/trypsin digestion (enzyme ratio: 1/100), and desalting as previously described (Yamana et al., 2013). The resulting peptides were labeled with isobaric tags for relative and absolute quantification (iTRAQ, Sciex) and mixed in loading buffer (0.5% trifluoroacetic acid and 4% (v/v) acetonitrile). They were subsequently subjected to NanoLC-MS/MS using a TripleTOF 5600 System (AB Sciex) equipped with an HTC-PAL autosampler (CTC Analytics). Loaded peptides were separated on a self-pulled analytical column (150-mm length, 100-μm i.d.) using a Dionex UltiMate 3000 RSLCnano System. The mobile phases were composed of 0.5% acetic acid with 5% (v/v) DMSO (solution A) and 0.5% acetic acid in 80% (v/v) acetonitrile with 5% (v/v) DMSO (solution B) (Hahne et al., 2013). A three-step gradient condition of 5%–10% (v/v) solution B for 5 min,

10%–40% (v/v) solution B for 60 min, and 40%–100% (v/v) solution B for 5 min was used at a flow rate of 400 μL/min. The applied spray voltage was 2,300 V, and the mass spectroscopy scan range was 300-1,500 m/z every 0.25 s. Analyses were performed in triplicate per sample, and blank runs were inserted between samples.

The raw data files were analyzed using ProteinPilot v5.0 (Sciex). Peak lists, which were generated from a ProteinPilot.group file, were analyzed using Mascot v2.5 (Matrix Science). Both database search engines were used against UniProt/Swiss-Prot release 2016_06 (8-June-2016) with previously described parameters (Yamana et al., 2013), except for a precursor mass tolerance of 20 ppm and a fragment ion mass tolerance of 0.1 Da for the search. For protein identification, peptides were grouped into protein groups based on previously established rules (Nesvizhskii and Aebersold, 2005). At least two confidently identified peptides per protein were used for the protein identification. In addition, a minimum peptide length of 6 amino acids and single peptides with higher confidence ($p < 0.01$) were allowed for the protein identification. False discovery rates (FDRs) were estimated by searching against a decoy sequence database (< 1%). The accumulated intensity of each iTRAQ label above a certain threshold was used for the ratio calculation for each protein.

QUANTIFICATION AND STATISTICAL ANALYSIS

Statistical Analysis

All statistical analyses were performed using GraphPad Prism software. To determine statistical significance, unpaired two-tailed Student's t test was used, except for bleeding time of mice and for platelet productivity in the micro fluidic system, for which Mann Whitney and Dunnett's test were used, respectively. The exact numbers for each "n" are provided and defined within the corresponding figures or figure legends. Data are shown as mean ± SD as indicated in the figure legends. Significance was assumed with $*p < 0.05$, $**p < 0.01$, $***p < 0.001$.

DATA AND SOFTWARE AVAILABILITY

The accession number for the microarray data reported in this paper is NCBI Gene Expression Omnibus: GSE112512. The dataset identifier for the MS/MS data reported in this paper is ProteomeXchange Consortium (http://proteomecentral.proteomexchange.org) via the jPOSTrepo (https://repository.jpostdb.org/): PXD009739 (JPST000418) (Okuda et al., 2017).

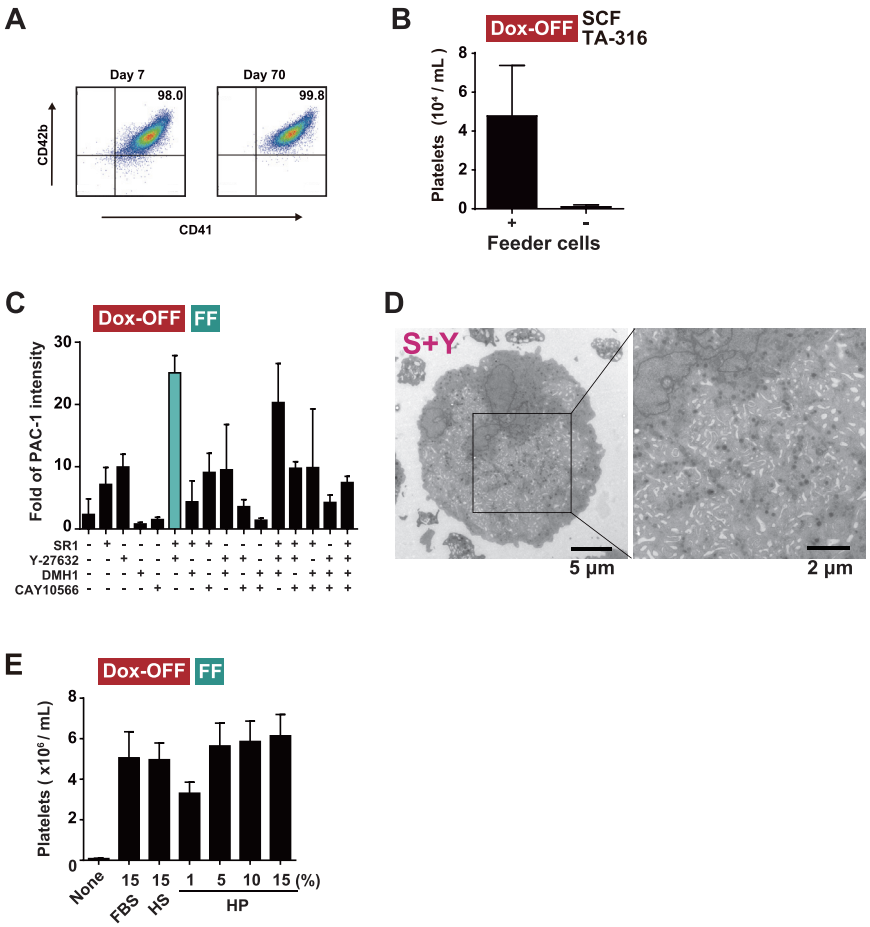

Figure S1. Establishment of Feeder-Independent Scalable Expansion and Maturation of imMKCLs, Related to Figure 1.

(A) Expression level of megakaryocyte surface markers on imMKCLs. During Dox-ON stage, imMKCL cell density was maintained at less than 2 × 10^6 per mL in a Petri dish by passaging with fresh cocktail A. Dot plots from flow cytometric analyses show the expression of CD41a (x axis) and CD42b (y axis) on days 7 and 70.

(B) Numbers of $CD41a^+CD42b^+$ platelets from Dox-OFF stage imMKCLs with or without C3H10T 1/2 feeder cells were evaluated on day 6. Cultivation was done by Dox-OFF medium with cocktail B and without SR-1 or Y-27632. n = 3 experiments.

(C) PAC-1 binding to platelets stimulated with 100 μM ADP and 40 μM TRAP-6, a hallmark of platelet activation, was evaluated in each platelet sample. Platelets were obtained by several protocols with SR1, Y27632, DMH1, and/or CAY10566 along with TA316, SCF, and KP457. n = 3 experiments.

(D) High-magnification TEM images of the imMCKLs shown in Figure 1F.

(E) Numbers of $CD41a^+CD42b^+$ platelets from Dox-OFF stage imMKCLs with cocktail B were evaluated. HS, human serum; HP, human plasma; FBS, fetal bovine serum. n = 3 experiments.

All data in B, C and E are means ± S.D.

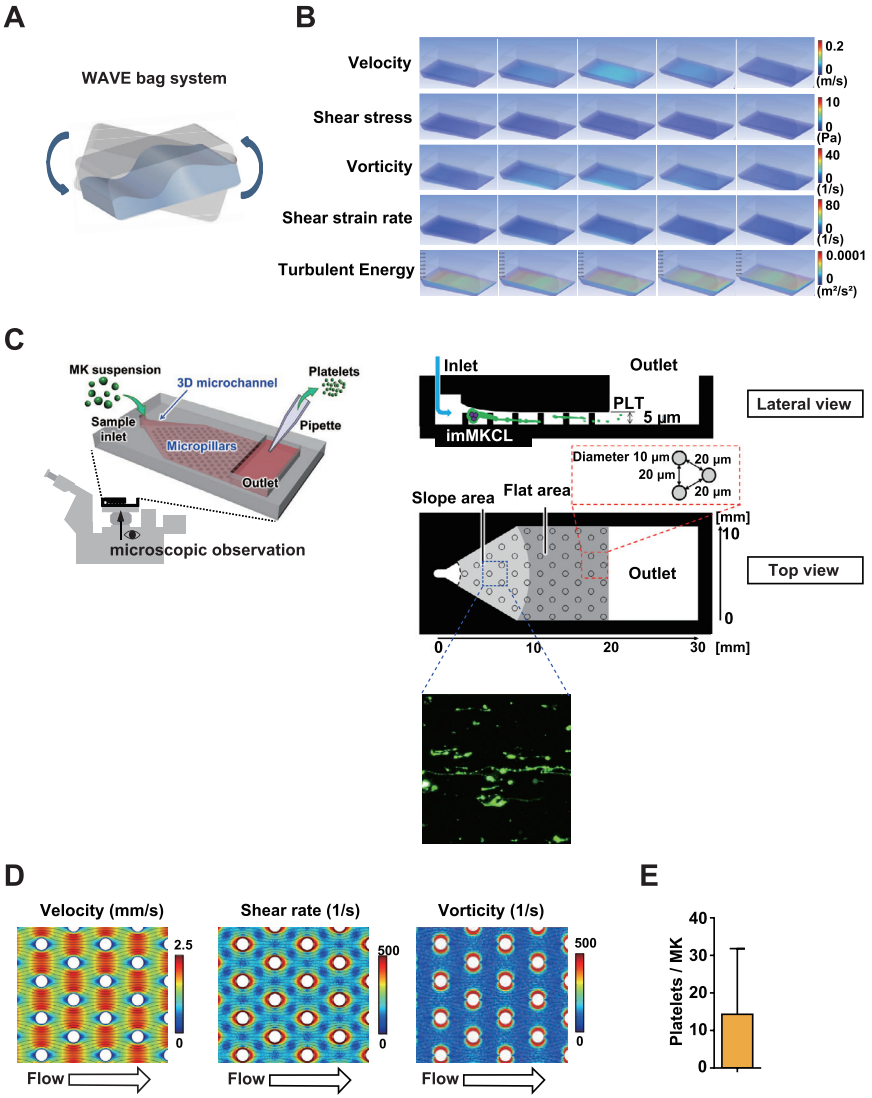

Figure S2. WAVE Bag System and a Newly Developed Microfluidic Chip as Bioreactors of Platelet Biogenesis, Related to Figure 2

(A) Schema of rocking incubation in the WAVE bioreactor.

(B) Physical parameters in the WAVE bioreactor: velocity (mm/s), shear stress (Pa), vorticity (1/s), shear strain rate (1/s), and turbulent energy (m^2/s^2). The parameters were calculated by simulation.

(C) Illustration of the microfluidic chip design. The width, depth, and height of the microfluidic chip were 40 mm, 15 mm, and 1.6 mm, respectively. The chip contained numerous pillars (diameter: 10 μm) at 20 μm intervals within the microchannel. Day 5 Dox-Off stage imMKCLs supplemented with cocktail B were applied into the inlet, and platelets were collected from the outlet. Representative image of proplatelets derived from GFP-expressing imMKCLs in the microfluidic chip is shown (lower panel; × 100).

(D) Simulation results of velocity (mm/s), shear rate (1/s), and vorticity (1/s) in the flat area of the microfluidic device under flow. The color bar shows the shear rate with a maximum value of 500 s^{-1} to improve visibility of the figure.

(E) Number of $CD41a^+CD42b^+$ platelets generated from imMKCLs is shown. Means ± S.D., n = 4 experiments. MK, megakaryocytes.

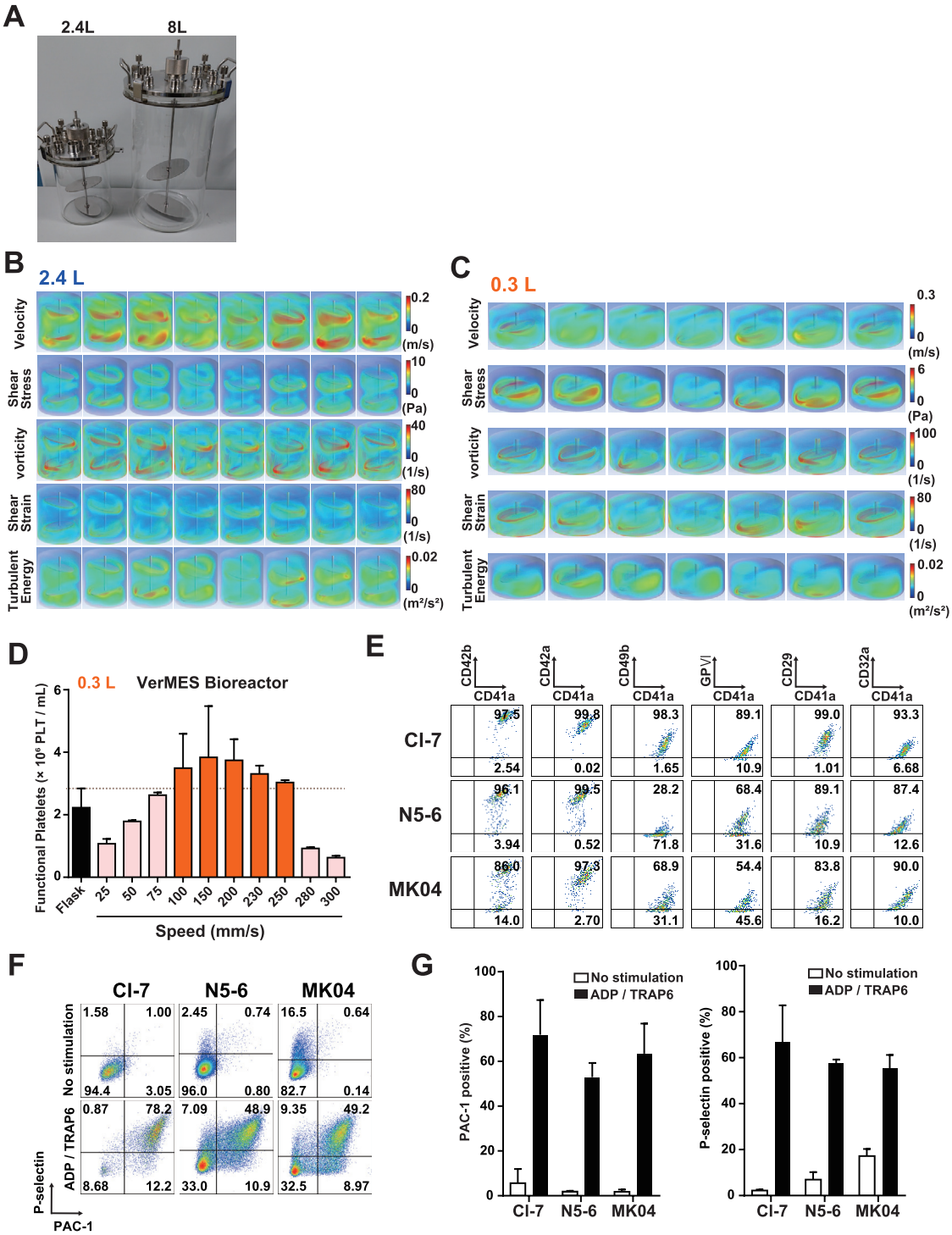

Figure S3. Optimal Shear Stress and Turbulent Energy in the VerMES Bioreactor Enables Scalable Platelet Biogenesis, Related to Figure 3

(A) Picture of 2.4 L and 8 L VerMES bioreactor vessels. Two oval shape blades are placed horizontally and in right angles to each other.

(B) Simulation results during 1 cycle of reciprocal motion with the indicated physical parameters in 2.4 L VerMES bioreactor.

(C) Simulation results during 1 cycle of reciprocal motion with the indicated physical parameters in 0.3 L VerMES bioreactor.

(D) Platelet yield from imMKCLs in a 25 mL shaking flask or 0.3 L VerMES with 15 mm strokes at the indicated speeds. The orange bars indicate speeds for VerMES (mean + SD) that surpassed platelet generation in a flask (dotted line). n = 3 to 15 experiments.

(legend continued on next page)

(E) Representative dot plots of flow cytometric analyses of various platelet antigens on donor platelets or iPSC-platelets produced in 8 L VerMES bioreactor for the indicated imMKCL clones. n = 3 experiments.

(F and G) Representative dot plots (F) and compiled data (G; mean ± SD) of flow cytometric analyses of PAC-1 binding and P-selectin expression with or without ADP/TRAP6 stimulation (100 μM ADP and 40 μM TRAP-6) on iPSC-platelets produced by 8 L VerMES bioreactor for the indicated imMKCL clones (× 630). n = 3 experiments.

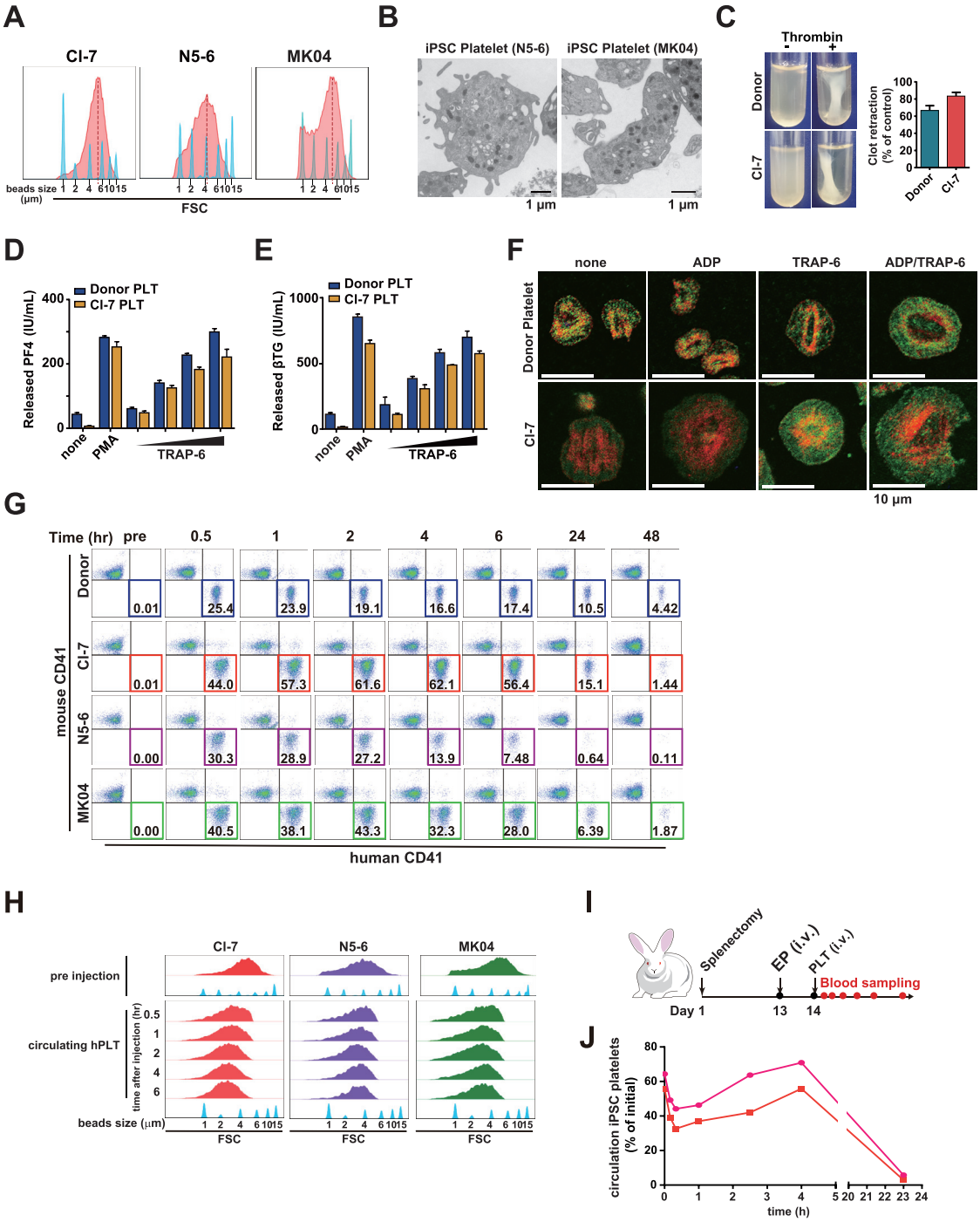

Figure S4. iPSC-Platelets Generated in the VerMES Bioreactor Improved Thrombotic Responses *In Vitro* and *In Vivo*, Related to Figure 4

(A) Size distribution of platelets derived from three imMKCL clones. Blue histograms represent size calibration beads with diameters of 1, 2, 4, 6, 10 or 15 μm. Red histograms represent $CD41^{+}CD42b^{+}$platelets, and red dotted lines indicates peak size. n = 3 to 4 experiments.

(B) TEM images of platelets derived from imMKCL clones N5-6 and MK04. Scale bars: 1 μm.

(C) Representative images and clot retraction rate by weight from clot retraction assays. n = 3 to 4 experiments.

(D and E) Release of platelet factor 4 (PF4) (D) or β-thromboglobulin (βTG) (E) from imMKCL Cl^{-}7-derived platelets (Cl^{-}7 PLT) or donor platelets following platelet activation was measured by ELISA. Samples were stimulated with PMA (0.2 μM) or TRAP-6 (5 to 40 μM, two fold increments). n = 3 experiments.

(F) Cl^{-}7-derived platelets were spread on fibrinogen-coated cover glass in the absence or presence of ADP (200 μM) and/or TRAP-6 (40 μM). Scale bars: 10 μm.

(G) Representative dot plots from flow cytometry data of mouse peripheral blood in Figure 4F. Squared areas indicate human CD41 positive platelets. Numbers indicate percentage of total platelets.

(legend continued on next page)

(H) CD41^{+}platelets size distribution before injection and in circulation in mouse peripheral blood after the indicated times. Blue histograms: beads size.
(I) Schema of a rabbit circulation model.
(J) The time course of circulating Cl^{-}7-derived platelets in two rabbits. Ratios of circulating platelets were calculated from an infused dose set at 100%.
All data in C-E are means ± S.D.

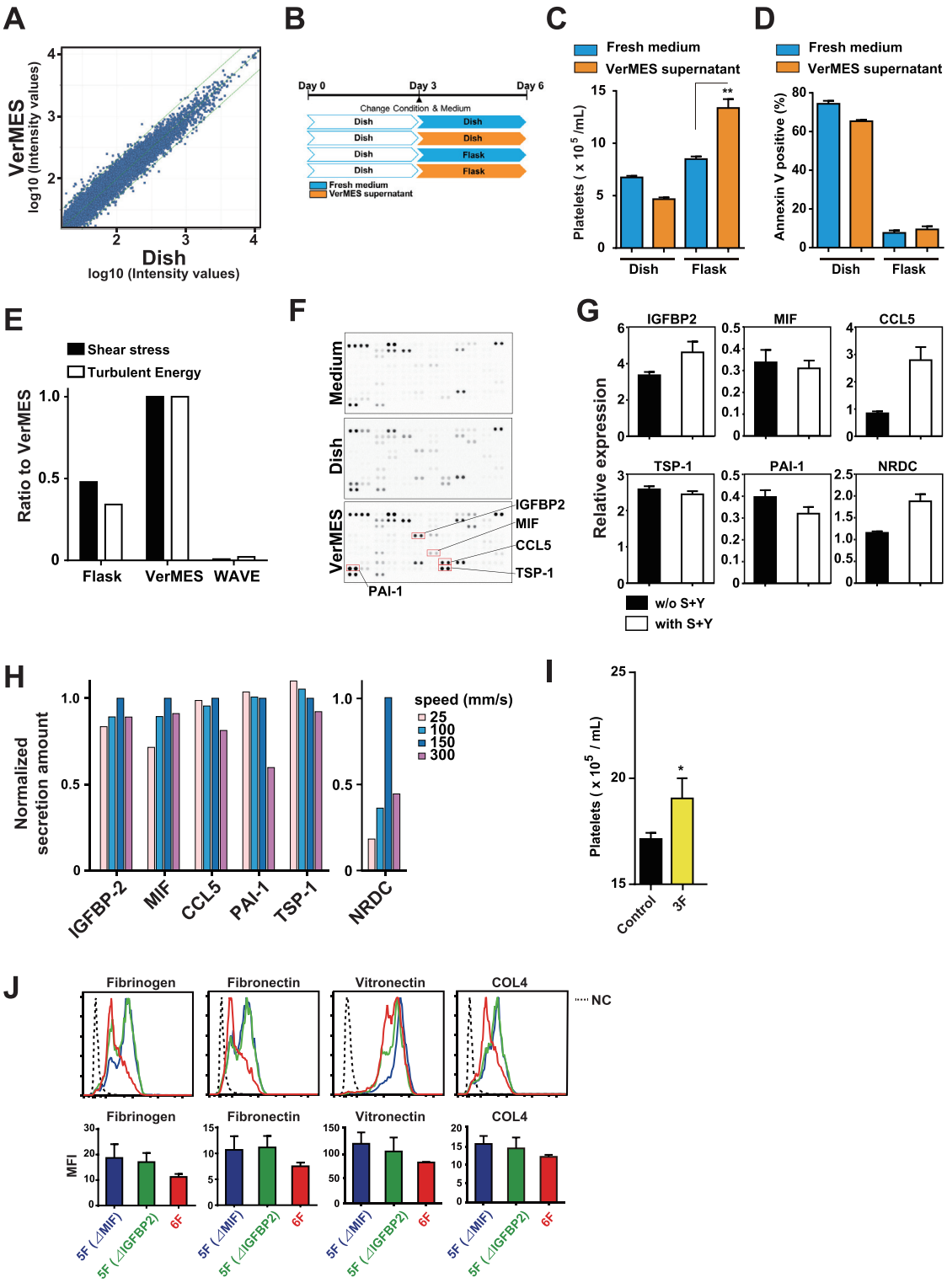

Figure S5. VerMES Cultivation Induced Release of Thrombopoietic Factors from imMKCLs, Related to Figure 5

(A) Scatterplot of gene expression in Dox-OFF stage imMKCL on day 3 between static dish and VerMES conditions. Diagonal lines indicate two-fold change.

(B) Schema of the experiment. imMKCLs were cultured for 3 days in a static dish with Dox-OFF medium, then 3 more days in a static dish or shaking flask with fresh or conditioned medium.

(C) Numbers of platelets from imMKCLs in the conditions described in (B). n = 3 experiments. **p < 0.01.

(legend continued on next page)

(D) Annexin V binding to iPSC-platelets in the conditions described in (B). n = 3 experiments.
(E) Relative ratio of shear stress (Pa) and turbulent energy (m^2/s^2) between 25 mL flask, 2.4 L VerMES, and 20 L WAVE. Values in VerMES were set to 1.0.
(F) Protein array analysis images with fresh medium and cocktail B and the day 4 culture supernatants of Dox-OFF stage imMKCLs under static conditions in a Petri dish on day 4 or in VerMES on day 4.
(G) Expression levels of IGFBP2, MIF, CCL5, TSP-1, PAI-1, and NRDC mRNA in Dox-OFF stage imMKCLs with or without SR1 (S) and Y-27632 (Y). Gene expression levels were normalized to GAPDH expression. n = 3 experiments.
(H) Similar to Figure 5A with 0.3 L VerMES but under different speed settings. The 150 mm/s setting was set to 1.0. y axis indicates the normalized secretion of individual proteins.
(I) Numbers of $CD41a^+CD42b^+$ platelets generated from Dox-OFF stage imMKCLs cultured for 3 days in the presence of cocktail B in a dish and transferred to shaking flasks with the administration of three recombinant factors (NRDC, IGFBP-2, MIF) or none (Control) and incubated for another 3 days. n = 3 experiments. $^*p < 0.05$.
(J) Similar to Figure 5G, Dox-OFF stage imMKCLs were cultured for 4 days in the presence of cocktail B in a dish. After incubating for an additional 24 h in a shaking flask, 6F, 5F (ΔIGFBP2), and 5F (ΔMIF) conditions were compared. Representative histograms are shown for the expression levels of fibrinogen, fibronectin, vitronectin, and collagen IV. Dotted lines in the histograms indicate negative control. x axis, fluorescence intensity (log scale); y axis, cell counts. In the bar graphs, MFI results are shown as means ± S.D. n = 3 experiments.
All data in C, D, G, I and J are means ± S.D.

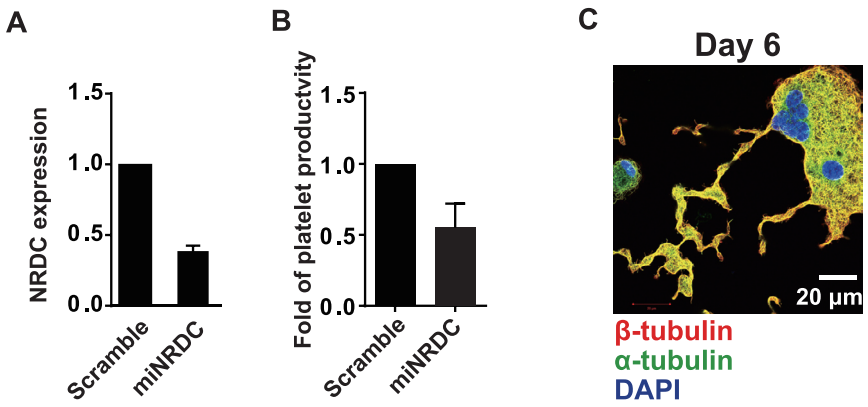

Figure S6. NRDC Contributes to Platelet Production in Extracellular Space and Intracellular Compartment, Related to Figure 6

(A) Relative expression levels of total NRDC mRNA in imMKCLs exposed to control scramble miRNA or active inhibitory miRNA construct against NRDC (miNRDC). Gene expression was normalized to GAPDH expression. The scramble was set to 1.0 in individual samples. n = 3 experiments.

(B) Numbers of $CD41a^{+}CD42b^{+}$ platelets detected in the culture of imMKCL treated with scramble miRNA or miNRDC. n = 3 experiments.

(C) Confocal micrographs of mature imMKCLs spread on a fibronectin-coated cover glass on day 6 (× 630). The cells were fixed, permeabilized and stained for α-tubulin (green), β1-tubulin (red), and DAPI (blue). Scale bar: 20 μm.

All data in A and B are means ± S.D.